



# Water vapour isotopes over West Africa as observed from space: which processes control tropospheric H<sub>2</sub>O/HDO pair distributions?

Christopher J. Diekmann<sup>1,a</sup>, Matthias Schneider<sup>1</sup>, Peter Knippertz<sup>2</sup>, Tim Trent<sup>4,5</sup>, Hartmut Boesch<sup>4,c</sup>, Amelie Ninja Roehling<sup>1</sup>, John Worden<sup>6</sup>, Benjamin Ertl<sup>1,3</sup>, Farahnaz Khosrawi<sup>1,b</sup>, and Frank Hase<sup>1</sup>

<sup>1</sup>Institute of Meteorology and Climate Research, Atmospheric Trace Gases and Remote Sensing, Karlsruhe Institute of Technology, Karlsruhe, Germany

<sup>2</sup>Institute of Meteorology and Climate Research, Department Troposphere Research, Karlsruhe Institute of Technology, Karlsruhe, Germany

<sup>3</sup>Steinbuch Centre for Computing, Karlsruhe Institute of Technology, Karlsruhe, Germany

<sup>4</sup>Earth Observation Science, Department of Physics and Astronomy, University of Leicester, Leicester, UK

<sup>5</sup>National Centre for Earth Observation, Department of Physics and Astronomy, University of Leicester, Leicester, UK

<sup>6</sup>Jet Propulsion Laboratory, California Institute of Technology, Pasadena, California, USA

<sup>a</sup>now at: Telespazio Germany GmbH, Darmstadt, Germany

<sup>b</sup>now at: Jülich Supercomputing Centre, Forschungszentrum Jülich GmbH, Jülich, Germany

<sup>c</sup>now at: Institute of Environmental Physics, University of Bremen, Bremen, Germany

**Correspondence:** Christopher J. Diekmann (chjdiekmann@gmail.com)

**Abstract.** The West African Monsoon (WAM) represents the main source of rainfall over West Africa and thus has important socio-economic impacts. However, the complex interactions of the large-scale circulation, convective dynamics and microphysical processes pose a substantial challenge to reliably quantify the atmospheric branches of the hydrological cycle in observations and models.

- 5 Making use of recent advances in retrieving the isotopic composition of tropospheric water vapour from space, we promote the paired analysis of H<sub>2</sub>O and HDO to investigate the moisture pathways and processes associated with the WAM. Data from the state-of-the-art satellite sensors IASI, AIRS and TROPOMI, together with the multi-satellite IMERG precipitation product, serve to characterize the variability of H<sub>2</sub>O and HDO (with their ratio product  $\delta D$ ) over West Africa from a convective as well as seasonal perspective and with respect to impacts from dynamical and microphysical processes. In particular, we find:
- 10 (1) Monsoon convection over the Sahel leads to a marked anti-correlation between increasing H<sub>2</sub>O and decreasing  $\delta D$  in the free troposphere. This is due to strong dry air intrusions from the Saharan upper troposphere that feed into Sahelian squall line systems, foster rain evaporation and, hence, lead to  $\delta D$  depletion; (2) Over the Guinea Coast, convective precipitation is associated with overall moist and enriched signals without showing significant  $\delta D$  depletion. Here, surface evaporation from the Tropical Atlantic moistens the troposphere, reducing the efficiency of the rain evaporation and the corresponding  $\delta D$  depletion;
- 15 (3) During the Sahelian monsoon peak, an anti-correlation between increasing precipitation amount and decreasing  $\delta D$  becomes apparent. Thus, this provides observational evidence for the amount effect in tropospheric water vapour, similar to what is known for the isotopic composition in precipitation; (4) When no considerable precipitation occurs, e.g. during the Sahelian winter, the {H<sub>2</sub>O,  $\delta D$ } signals point to dry air mass mixing from large-scale circulation.

This study demonstrates that different microphysical and dynamical processes occurring over West Africa leave distinct fea-



20 tures in the isotopic composition of water vapour, and, hence, underlines the overall value of using paired  $\text{H}_2\text{O}$  and  $\delta\text{D}$  obser-  
vations from space to study effects of processes that control tropical convection.

## 1 Introduction

The West African Monsoon (WAM) is one of the most prominent atmospheric features of the West African climate system (Fink et al., 2017). Over the semi-arid Sahel zone, the WAM causes a pronounced annual cycle that ranges from very dry  
25 winter months, when northeasterly Harmattan winds from the Sahara dominate, to a marked rainy season during summer, when southwesterly monsoon winds transport moisture from the Tropical Atlantic into the Sahel and feed intense convective  
rainfalls, often related to westward propagating squall lines (Lafore et al., 2017). With the WAM thus being the main source  
of annual precipitation over the Sahel (Dhonneur, 1981; Fink et al., 2006), its socio-economic impacts are enormous, as the  
region heavily relies on rain-fed agriculture (Sultan et al., 2005; Berntell et al., 2018). From a climatological perspective,  
30 changes in the WAM system are critical, e.g. for the degree of desiccation (Hulme, 2001) and contribution to the greenhouse  
effect (Spencer and Braswell, 1997) of West Africa. In addition, the WAM system is also found to affect weather systems in  
remote areas through dynamical teleconnections, such as over the North Atlantic and Europe (Bielli et al., 2010; Gaetani et al.,  
2011; Pante and Knippertz, 2019).

The simulation of the atmospheric processes related to the WAM, however, still poses a major challenge for modern numer-  
35 ical weather and climate models (Roehrig et al., 2013; Vogel et al., 2018). This is mainly due to the strong non-linearity in the  
coupling of atmospheric circulation, radiative transfer, land surface features, boundary layer processes as well as microphysical  
processes associated with convection (e.g. Colman et al., 2017; Lafore et al., 2017). Even a seemingly accurate precipitation  
forecast may be a result of error compensation within the model, with the effect of potentially reducing the robustness of  
climate projections using this model. Studies have shown that the main source of uncertainty in this context is convection,  
40 mostly due to insufficient spatio-temporal resolution and the poor simulation of the convective organization and interaction  
with its environment (Marsham et al., 2013; de Vries et al., 2022). In particular convective mixing processes play a crucial role  
in controlling the free tropospheric water vapour budget, which in turn affects the radiative transfer and atmospheric stability,  
but accurately simulating these processes can be particularly challenging. In addition, the network of observations is limited  
in West Africa (Parker et al., 2008) and may not be adequate to capture the effects of the controlling processes required to  
45 enhance our general process understanding and to improve model performance.

A promising approach to provide new insights into different branches of the hydrological cycle and to validate numerical  
models is to inspect the isotopic composition of water in the atmosphere, in all its forms: liquid, gaseous and solid. As each  
water isotopologue (in the following, referred to as water isotope) is associated with characteristic binding energies and diffu-  
sivities, the ratios of different isotope concentrations are altered during phase changes. In this way, paired distributions of the  
50 light water isotope  $\text{H}_2\text{O}$  against heavier molecules such as HDO can be used to track effects from microphysical and dynamical  
processes and thus reveal unique insights into the history of observed air masses (e.g. Worden et al., 2007; Noone et al., 2011;  
Noone, 2012; Bolot et al., 2013; Galewsky et al., 2016; González et al., 2016; Schneider et al., 2016; Lacour et al., 2018; Risi



et al., 2021). Typically, the ratio between HDO and H<sub>2</sub>O is given in the  $\delta D$  notation (in ‰) with respect to the standardized ratio  $R_s = 3.1152 \times 10^{-4}$  (Craig, 1961):

$$55 \quad \delta D = \left( \frac{\text{HDO}/\text{H}_2\text{O}}{R_s} - 1 \right) \cdot 1000, \quad (1)$$

and concomitant distributions of H<sub>2</sub>O and  $\delta D$  are often referred to as {H<sub>2</sub>O,  $\delta D$ } pairs.

Previous studies have investigated tropospheric distributions of stable water isotopes during the WAM using campaign-based observations of near-surface humidity (Risi et al., 2008b, 2010a; Tremoy et al., 2012, 2014), spatio-temporally limited retrievals from historical space-borne sensors (Risi et al., 2010b) and isotope-enabled atmospheric models (Risi et al., 2010a; 60 Diekmann et al., 2021a; Risi et al., 2023). These studies underline the strong influence of large-scale dynamics and microphysical processes on the isotopic composition of rain and water vapour. In particular, partial evaporation of falling rain droplets in the boundary layer and free troposphere has been linked to convective systems such as squall lines, and was found to account for an increased depletion of  $\delta D$  observed in both liquid hydrometeors and ambient vapour. By applying a model-based Lagrangian process attribution Diekmann et al. (2021a) confirmed in a reverse engineering approach that the paired {H<sub>2</sub>O,  $\delta D$ } 65 phase space is particularly suited to represent effects of the main atmospheric processes controlling the WAM. They found that its isotopic signatures in the troposphere during the summer monsoon period are well-explained by means of theoretical formulations derived by Noone (2012): (1) dynamical processes, in particular the mixing of moist air masses from the Tropical Atlantic with dry air from the Sahara affected by large-scale subsidence, and (2) microphysical processes, namely condensation and evaporation equilibration of liquid hydrometeors. In order to evaluate these theoretical concepts with real observations, 70 new tropospheric datasets of pairs of H<sub>2</sub>O and  $\delta D$  with dense spatio-temporal coverage are needed, which, however, have only recently become available for West Africa.

Despite its smaller abundance compared to other heavy isotopes in atmospheric water vapour molecules, deuterium has distinct spectroscopic features in the infrared electromagnetic range, allowing detection and quantification from remote sensing sensors (Clerbaux et al., 2009). With recent advances in the development of retrieval processors for state-of-the-art satellite 75 sensors in terms of computational efficiency and data storage, new spaceborne datasets of tropospheric {H<sub>2</sub>O,  $\delta D$ } pairs with high spatio-temporal coverage over multiple years have become available. For instance, corresponding retrievals were performed for observations on daily and global basis from the current infrared sensors Metop/IASI (Infrared Atmospheric Sounding Interferometer; Schneider et al., 2012, 2022; Diekmann et al., 2021b), Aqua/AIRS (Atmospheric Infrared Sounder; Worden et al., 2019) and Sentinel-5P/TROPOMI (Tropospheric Monitoring Instrument; Schneider et al., 2020; Trent et al., 80 2021). The growing availability of such datasets creates new opportunities for investigating atmospheric moisture processes from convective to climatic scales.

In this study, we make use from the high spatio-temporal coverage given by the {H<sub>2</sub>O,  $\delta D$ } pair datasets from IASI, AIRS and TROPOMI in order to investigate the isotopic signatures of tropospheric water vapour over West Africa. Building on an observational basis, the aim is to shed new light on atmospheric processes governing the WAM development, in particular on 85 microphysical processes associated to convection and on the impact from large-scale circulation. The focus will be on:

- effects of convection in the {H<sub>2</sub>O,  $\delta D$ } phase space on a daily event basis,



**Table 1.** Remote sensing datasets used within this study, sampled for the region of interest over West Africa ( $0^{\circ} - 15^{\circ}$  N,  $8^{\circ}$  W –  $8^{\circ}$  E).

Platform	Data Product	Hor. Res.	Local Overpass	Data Availability
IASI	{H <sub>2</sub> O, δD} profiles	12 km	09.30 and 21.30	Jan 2015 – Dec 2020
AIRS	{H <sub>2</sub> O, δD} profiles	13.5 km	13.30	Jan 2015 – Dec 2019
TROPOMI	{H <sub>2</sub> O, δD} total columns	5.5 – 7 km	13.30	Apr 2018 – Dec 2020
IMERG	half-hourly prec.	0.1°	-	Jun – Jul 2016, 2018 – 2020
	monthly mean prec.			Jan 2018 – Dec 2020

- the interannual seasonal variability of convection-related {H<sub>2</sub>O, δD} signals,
- the quasi-climatological seasonal cycle of {H<sub>2</sub>O, δD} signals.

For this purpose, this study also includes the hourly precipitation rates from the multi-satellite precipitation product IMERG (Integrated Multi-Satellite Retrievals for GPM; Huffman et al., 2014) to link the observed {H<sub>2</sub>O, δD} pair signals to the prevailing precipitation conditions. We further utilize the IMERG data to detect individual major convective events as well as pronounced dry periods, with the aim to identify the corresponding {H<sub>2</sub>O, δD} observations and inspect the isotopic signatures for the different conditions. In order to foster the process-based understanding of the observed {H<sub>2</sub>O, δD} pair signals, we add the theoretical process curves from Diekmann et al. (2021a) to assess effects from rain-vapour interactions and large-scale circulation to the {H<sub>2</sub>O, δD} phase space.

The paper is structured as follows: Section 2 documents the research datasets and analysis methods considered throughout this study. We analyze the remote sensing data for different target regions over West Africa on the convective scale (Sect. 3), with respect to the year-to-year variability (Sect. 4) and with a focus on the mean seasonal cycle (Sect. 5). The main conclusions and an outlook are given in Sect. 6.

## 100 2 Data and Methods

With the aim to characterize and further understand the {H<sub>2</sub>O, δD} pair variability over West Africa, this study makes use of observational datasets from space-based remote sensing (see Table 1) in combination with additional interpretative frameworks (see Sect. 2.1 and see 2.2). Domains over the Guinea Coast and the Sahel serve as study regions with different climatological conditions and are defined in alignment with Knippertz et al. (2017), i.e. latitudinal bounds of  $0^{\circ}$  to  $7.5^{\circ}$  N and  $7.5^{\circ}$  to  $15^{\circ}$  N, respectively, with common longitudinal bounds of  $8^{\circ}$  W to  $8^{\circ}$  E. These domains are found to be useful for documenting the shift of maximum precipitation from the coastal to the Sahelian regions, which is a key criterion for defining the onset and further evolution of the WAM (Fitzpatrick et al., 2015; Knippertz et al., 2017; Diekmann et al., 2021a).

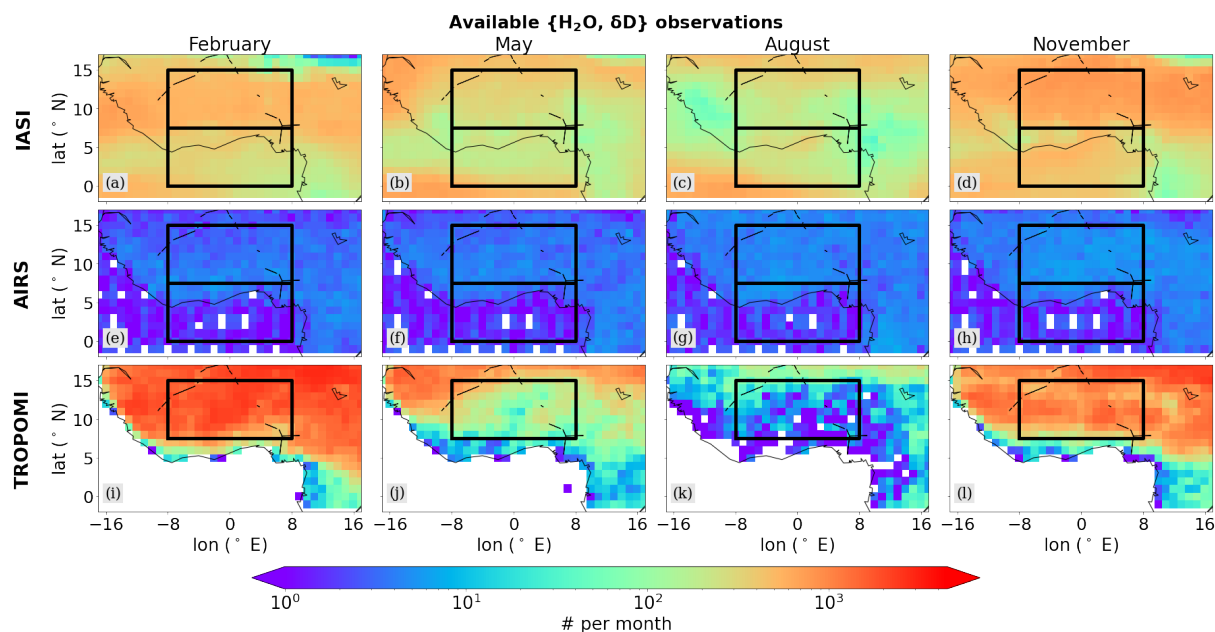


**Figure 1.** Horizontal distributions of the monthly averaged (from left to right February, May, August, November) coverage of available isotope retrievals from IASI, AIRS and TROPOMI evaluated on a  $1^\circ \times 1^\circ$  grid, after filtering for clouds and data quality. The black frames indicate the study regions over the Sahel (upper box) and the Guinea Coast (lower box). As the TROPOMI dataset only consists of observations over land, the Guinea Coast region is omitted when studying the TROPOMI observations.

## 2.1 Tropospheric water isotope products from remote sensing

110 The main data sources for this study are three long-term and global datasets of tropospheric  $\{H_2O, \delta D\}$  observations that were  
 retrieved from state-of-the-art satellite sensors and made available in recent years (see Table 1). In the following we briefly  
 describe these products and highlight selected particularities that are relevant for this study. Due to the distinct spectroscopic  
 features of deuterium in the infrared spectrum, infrared sounders have been proven useful to retrieve HDO abundances in the  
 troposphere. However, water vapour products from these sensors are currently limited to cloud-free conditions, thus inducing  
 115 a dry bias in larger-scale water vapour distributions (Schneider et al., 2010).

The first water isotope product is the  $\{H_2O, \delta D\}$  pair dataset generated from thermal infrared spectra from Metop/IASI (Diek-  
 mann et al., 2021b; Schneider et al., 2022), developed and published in the framework of the MUSICA project (Schneider  
 et al., 2012, 2016). This paired product is created using a post-processing step (1) to increase the sensitivity of the  $\delta D$  data in  
 particular for dry conditions and (2) to harmonize the vertical sensitivities of the retrieved  $H_2O$  and  $\delta D$  products, such that both  
 120 profiles are representative for the overall same altitude regions, i.e.  $H_2O$  and  $\delta D$  have matching averaging kernels (Wiegele  
 et al., 2014; Schneider et al., 2016; Barthlott et al., 2017; Diekmann et al., 2021b). The MUSICA IASI  $\{H_2O, \delta D\}$  pair product  
 is sensitive to variations of  $H_2O$  and  $\delta D$  in the free troposphere predominantly at around 4.2 km, with contributions from layers



up to 2–6 km (800–400 hPa). Diekmann et al. (2021b) have reported typical errors of up to  $\sim 12\%$  for  $\text{H}_2\text{O}$  and  $30\%$  for  $\delta\text{D}$  at 4.2 km. The constellation of at least two simultaneously operating Metop satellites allows to achieve a twice daily global coverage, with equator crossings at around 09:30 and 21:30 local time. Here, we consider only quality-checked  $\{\text{H}_2\text{O}, \delta\text{D}\}$  pair data according to the recommended filter conditions for observations with high sensitivity, as defined in Diekmann et al. (2021b).

The second product is the corresponding dataset from the Aqua/AIRS sensor (Worden et al., 2019). Similar to IASI, it captures the thermal infrared part of the Earth's outgoing radiation, thus, analogously its  $\{\text{H}_2\text{O}, \delta\text{D}\}$  product is also most sensitive to water isotope abundances in the free troposphere. For the scope of this study  $\{\text{H}_2\text{O}, \delta\text{D}\}$  data with a sensitivity peak between 825 and 421 hPa are selected. Errors reported for  $\delta\text{D}$  are in a similar range as for IASI ( $\sim 25 - 30\%$ ). Conceptually, the overall AIRS retrieval processor shares similarities with the MUSICA IASI retrieval, with however the difference that it deploys no additional post-processing to achieve harmonization of the averaging kernels of the  $\text{H}_2\text{O}$  and  $\delta\text{D}$  retrieval states. In particular for dry conditions, the retrieval results were found to be much more sensitive to variations in  $\text{H}_2\text{O}$  than in  $\delta\text{D}$ , with the effect that the averaging kernels of  $\text{H}_2\text{O}$  and  $\delta\text{D}$  showed significant discrepancies in their vertical structures. This might have the consequence that the retrieved  $\text{H}_2\text{O}$  and  $\delta\text{D}$  results evaluated at the same retrieval grid level may not represent the same air masses, so that their direct comparison would create misleading results. A more detailed discussion on these difficulties is given in Schneider et al. (2016).

A third product of tropospheric water isotope data is retrieved from the short-wave infrared sensor Sentinel-5P/TROPOMI and recently published in the scope of the ESA S5P+Innovation Water Vapour Isotopologues ( $\text{H}_2\text{O}$ -ISO) project by Trent et al. (2021). In contrast to IASI and AIRS, which capture infrared radiation emitted by the Earth's surface and atmosphere, TROPOMI measures solar radiation back-scattered at the Earth's surface. By making use of the TROPOMI observations only over land, where the back-scattering features of the short-wave infrared radiation are significantly more effective than over oceans, Trent et al. (2021) performed total-column-averaged dry-air mole fraction retrievals of  $\text{H}_2\text{O}$  and  $\text{HDO}$  ( $\delta\text{D}$  is then a posteriori calculated using Eqn.1). The uncertainty of the TROPOMI  $\delta\text{D}$  product is estimated to achieve values of up to  $\sim 30\%$ , thereby being comparable to IASI and AIRS. The total-column-averaged  $\delta\text{D}$  represents a weighted vertical  $\delta\text{D}$  average, with the weighting performed according to the vertical  $\text{H}_2\text{O}$  distribution, i.e. reported  $\delta\text{D}$  values are determined by the most humid atmospheric layers. Consequently, we expect the column-averaged  $\{\text{H}_2\text{O}, \delta\text{D}\}$  products from TROPOMI to overall reflect the isotopic composition of the boundary layer or, in case of the WAM, the monsoon layer (i.e. the near-surface humid layer during the monsoon, which is typically deeper than the actual boundary layer). Further, we apply the quality filtering and bias correction for  $\text{H}_2\text{O}$  and  $\delta\text{D}$  as described and suggested in Trent et al. (2021).

For the scope of this study, we make use of the  $\{\text{H}_2\text{O}, \delta\text{D}\}$  dataset from IASI for its currently available period of 2015–2020, thereby resulting in a data overlap of five year with AIRS (available until 2019) and of almost three years with TROPOMI (available from April 2018 until December 2020). Figure1 shows the mean data availability of the considered data products over West Africa. Overall, the  $\{\text{H}_2\text{O}, \delta\text{D}\}$  pair dataset from IASI has a robust good coverage with up to  $10^3$  observations per  $1^\circ \times 1^\circ$  grid box per month. Observation counts are highest in the drier months February and November and lowest during rainy August, in particular over the precipitation maximum along the western coast and in Nigeria. AIRS has a data coverage



comparably constant over time, however, with a significantly lower amount of available observations per grid point. In contrast to IASI and AIRS, TROPOMI data are available only over land, which is why we will omit the Guinea Coast domain for this sensor throughout this study. Further, a strong seasonal cycle in the data availability of TROPOMI becomes apparent, ranging from high to low data volumes from winter to summer. The fact that the reduced coverage correlates with the monsoon activity peak suggests that this is result of the cloud treatment in the TROPOMI retrieval processing.

As our study focuses on the information content of the retrieved water isotope observations and their implications on process understanding during the WAM, the reader interested in more technical information of the sensors and data products is encouraged to review the corresponding publications and documentations.

## 2.2 Precipitation products from remote sensing

In order to obtain information about precipitation over West Africa, we make use of the IMERG precipitation dataset, which is a fused product from precipitation estimates retrieved during the TRMM (Tropical Rainfall Measuring Mission) and GPM (Global Precipitation Mission) satellite missions (Huffman et al., 2014). The retrieved precipitation estimates are calibrated with actual rain gauge data on a monthly basis and the final IMERG precipitation product is available on a half-hourly and a monthly basis (Huffman et al., 2019). Using long-term series of several rain gauges, Maranan et al. (2020) have performed a systematic and process-based validation of the IMERG precipitation product for the West African zone and, hence, have demonstrated that IMERG is capable of reproducing the well-known evolution of West African precipitation over the full year. The high resolution in space and time of the remotely sensed  $\{H_2O, \delta D\}$  pairs from the sensors described in Sect. 2.1 allows to examine the impact of individual convective systems on tropospheric water isotope signals. As the considered IASI, AIRS and TROPOMI datasets are limited to cloud-free scenes, we cannot measure directly the impact of microphysical rain processes occurring within convective cells. Therefore, we utilize the IMERG precipitation dataset to derive a simple clustering method, which allows to assess, whether the observed cloud-free air masses have been affected in their recent history by convective precipitation. In this context, we aim to categorize the available satellite observations as follows: (1) If within a chosen grid box and at a given calendar day the hourly precipitation averaged per day and then summed over the previous three days remains below a chosen threshold (here,  $0.2 \text{ mm hr}^{-1}$ ), then all observations inside this grid box and at the target date are classified as *non-rain* observations. (2) If one day prior to the given calendar day a chosen grid box experiences an averaged precipitation rate higher than a chosen threshold (here,  $3 \text{ mm hr}^{-1}$ ), then all observations within this grid box and at the target date are classified as *post-rain*. For this purpose, we consider the half-hourly IMERG precipitation data to cluster the daily  $\{H_2O, \delta D\}$  pairs from all three sensors at a target grid size of  $1^\circ \times 1^\circ$ . Despite the rather simple nature of this approach (e.g. neglecting effects such as the advection of air masses from adjacent grid boxes), the current choice of thresholds proves successful to identify the targeted precipitation states, i.e. persistent dry conditions against convective systems with marked precipitation (see Sect. 3).

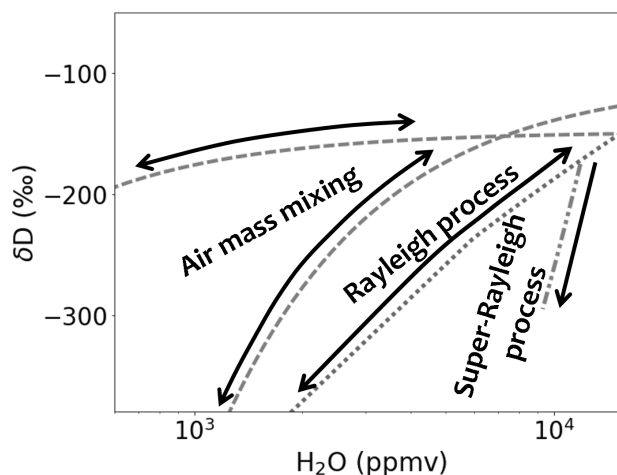


**Figure 2.** Theoretical process curves describing effects of idealized dynamical and microphysical processes in the  $\{H_2O, \delta D\}$  phase space. The curves are defined as described in Diekmann et al. (2021a).

### 2.3 Process curves in the $\{H_2O, \delta D\}$ phase space

190 Further, we make use of idealized process curves derived by Noone et al. (2011) that help interpret observed  $\{H_2O, \delta D\}$  pair distributions with respect to the underlying dynamical and microphysical processes. In particular, Diekmann et al. (2021a) have applied these process curves to describe characteristic  $\{H_2O, \delta D\}$  pair variations with respect to processes representative of the WAM (see Fig. 2): (1) The hyperbolic curves indicate characteristic  $\{H_2O, \delta D\}$  signals due to mixing of dry/depleted and humid/enriched air masses. (2) The diagonal Rayleigh lines mark the depletion in  $\delta D$  according to condensation and subsequent  
 195 moisture removal by rainout. If evaporation and equilibration occur on top of a Rayleigh process, then enhanced depletion in  $\delta D$  takes place and leads to the so-called Super-Rayleigh regime below the diagonal Rayleigh lines (3). This is found to be particularly pronounced over the Sahel during the WAM season, when well-organized convective systems such as squall lines lead to intense convective rainfall.

Throughout this study, the idealized curves identified in Diekmann et al. (2021a) will provide a process-based interpretation  
 200 context for the  $\{H_2O, \delta D\}$  pair variability as observed by the remote sensing sensors.

### 3 Convective-scale variability of $\{H_2O, \delta D\}$ pair signals

In a first step, we aim to address the variability of the spaceborne  $\{H_2O, \delta D\}$  pair observations with respect to microphysical processes that are associated with convection on a daily event basis. It applies the clustering method from Sect. 2.2 to the  $\{H_2O, \delta D\}$  data from IASI, AIRS and TROPOMI to identify those observations that were impacted by considerable monsoon  
 205 precipitation and to contrast them to largely dry instances. In the following, this is done for a case study focusing on the season



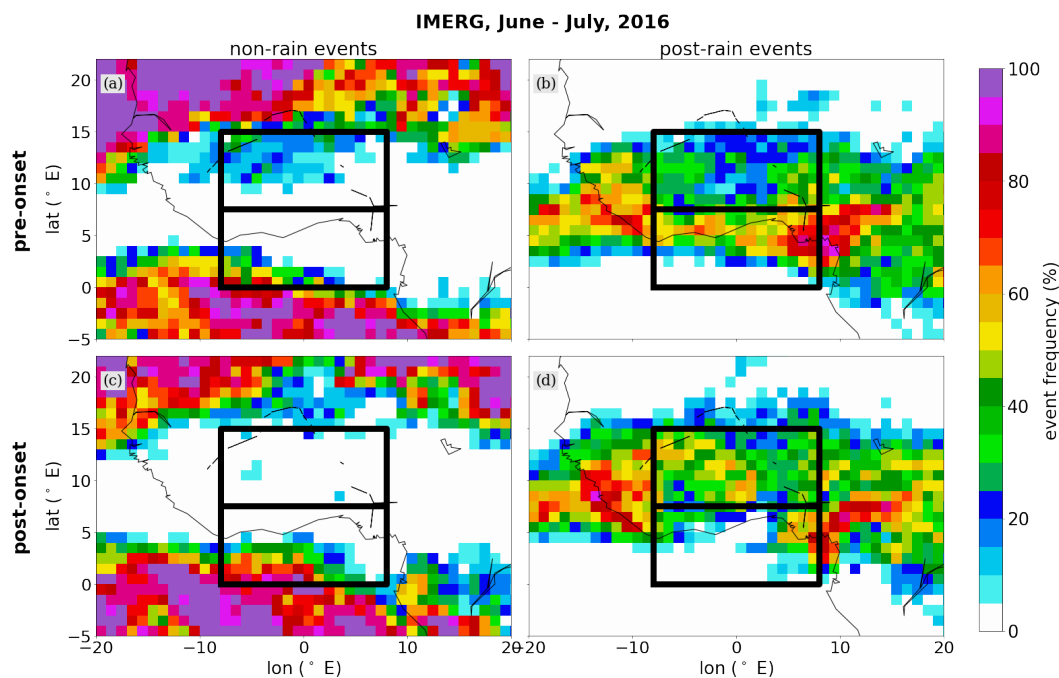


**Figure 3.** Fraction of days marked as (a, c) non-rain and (b, d) post-rain events for the pre- and post-onset phases of the WAM between June – July 2016 (with the monsoon onset occurred on 22 June 2016), derived by considering the daily averaged precipitation from the half-hourly IMERG precipitation dataset and evaluated on a  $1^\circ \times 1^\circ$  grid. The black-framed boxes depict the chosen target domains over the Guinea Coast and the Sahel.

2016 and additionally for a statistical multi-year analysis.

### 3.1 Rain analysis of West African Monsoon 2016

We demonstrate the basic concept of the clustering approach into *non-rain* and *post-rain* events and evaluate it on a case-study basis using the IASI data during the West African Monsoon in 2016. This specific monsoon season was the key subject of the multi-platform DACCWA campaign (Knippertz et al., 2017), where data were collected over the period June – July 2016 in order to characterize the monsoon system from synoptic, microphysical, dynamical and aerosol perspectives. In this framework, the onset of the monsoon activity was defined according to the northwards shift of precipitation from the Guinea Coast to the Sahel and was set to 22 June 2016. Based on this, we separate the period into the pre-onset (01 – 21 June 2016) and the post-onset phase (22 June – 31 July 2016), with the aim to further underline the impact of the WAM activity to the  $\{H_2O, \delta D\}$  pairs.

Figure 3 provides a horizontal overview about the relative fraction of days that are identified as non-rain or post-rain events during the pre- and post-onset phases, for each considered  $1^\circ \times 1^\circ$  grid box over West Africa. Overall, this clustering appears

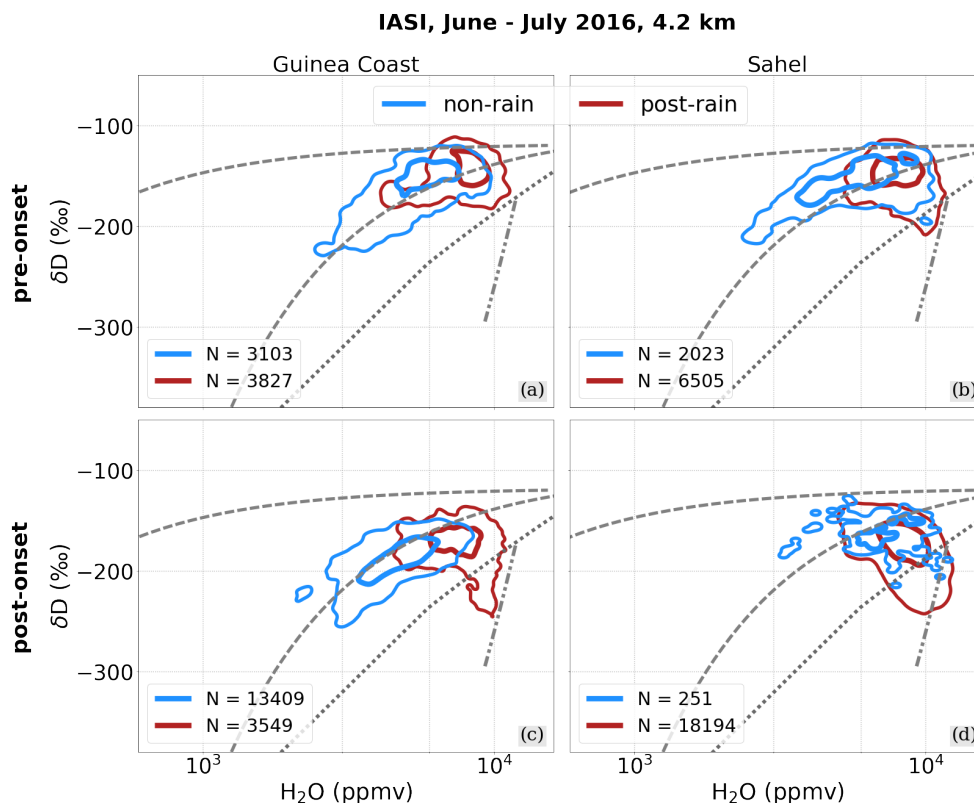


**Figure 4.** IASI  $\{H_2O, \delta D\}$  pair data over the Guinea Coast and the Sahel for the pre- and post-onset WAM phases between June – July 2016 (monsoon onset on 22 June 2016), clustered into non-rain and post-rain events based on daily averaged precipitation from IMERG. The  $\{H_2O, \delta D\}$  pair data are summarized by normalized two-dimensional histogram contours, with the contours indicating the main 90% and 50% of the respective data points and with the corresponding total data numbers given in the legend (calculated according to Eckstein et al. (2018)).

to successfully capture the areas associated with strong precipitation. It well reflects the onset criterion for the WAM activity, i.e. before the onset the predominance of precipitation is located over the Guinea Coast with occasional convective events over the Sahel, while after the onset the precipitation maximum moves to the Sahel. The post-onset phase leaves the Guinea Coast mostly rain-free with regional exceptions for its easternmost areas, where around the coasts of Nigeria and Cameroon, a localized and persistent precipitation peak prevails (e.g. discussed in Nlend et al., 2020).

Figure 4 shows the IASI  $\{H_2O, \delta D\}$  distributions sorted into non-rain and post-rain clusters for the phases before and after the monsoon onset. During the pre-onset phase, both regions feature a considerable number of events for both non- and post-rain classes. It becomes apparent that the non-rain events from both Guinea Coast and Sahel consistently evolve along the mixing line, which is in alignment with our understanding that no microphysical interactions have occurred and that the respective air masses are instead dominated by mixing. As discussed in the trajectory study from Diekmann et al. (2021a), air masses from



different origins meet over West Africa, mainly the moist southerly monsoon flow from the Gulf of Guinea, the dry Saharan  
230 northerly winds as well as dry intrusions from the upper troposphere.

As a response to the formation of strong precipitation systems over the Guinea Coast, we observe that the corresponding  
{ $H_2O$ ,  $\delta D$ } pairs mainly move upwards the mixing line to higher  $H_2O$  and  $\delta D$  regimes with no observable Rayleigh and  
Super-Rayleigh features. This can be explained by the fact that rain evaporation is reduced for more intense precipitation  
events (Dansgaard, 1964). As large rain drops fall faster, there is less time for evaporation, leading to less depletion of the  
235 ambient vapour (Stewart, 1975). Additionally, the rainfall over the Guinea Coast appears to be sufficiently large-scale and per-  
sistent such that the moist updrafts lead to a significant moistening of the free troposphere, which in turn leads to high relative  
humidity and thus further reduces the rain evaporation efficiency (Risi et al., 2008a; Lee and Fung, 2008; Yoshimura et al.,  
2010).

In contrast, over the Sahel a noticeable pull towards the rain-evaporation driven Super-Rayleigh regime stands out, forming a  
240 clearly anti-correlated relation between  $H_2O$  and  $\delta D$ . The precipitation events appear to be less intense than over the Guinea  
Coast (see Fig. 3), but over the Sahel strong intrusions from the Sahara and the upper troposphere transport dry and unsaturated  
air masses into the troposphere, hence increasing the rain evaporation efficiency. This effect intensifies during the post-onset  
phase, when precipitation is mainly driven by westward propagating convective events, so-called squall lines that induce strong  
convective precipitation in the leading edge of the system and moderate precipitation below the trailing stratiform cloud shield  
245 (e.g. Risi et al., 2008b, 2010b; Lafore et al., 2017; Diekmann et al., 2021a). The latter is characterized by smaller rain drops  
that, as discussed above, have in general a higher rain evaporation efficiency. Additionally, such squall line systems are driven  
by a rear-to-front inflow (usually connected to the African Easterly Jet), which feeds dry and unsaturated air to mid- and lower  
levels below the stratiform rain region and thus further increases the efficiency of rain evaporation. In this way, squall lines  
exert a strong fractionating effect on the West African troposphere, which is reflected in clear Super-Rayleigh features in the  
250 post-rain { $H_2O$ ,  $\delta D$ } pairs over the Sahel and slightly over the Guinea Coast after the monsoon has set in. This is in agreement  
with Diekmann et al. (2021a), who attributed this Super-Rayleigh regime to microphysical rain processes within the melting  
zone of a convective system, namely the evaporation of falling rain drops in unsaturated areas as well as the equilibration  
between water vapour and relatively depleted rain drops formed from melting snow for saturated conditions.

### 255 3.2 Multi-year analysis

After characterizing the predominant control processes of the IASI { $H_2O$ ,  $\delta D$ } pairs during June – July with respect to the mon-  
soon onset during 2016, the objective of this section is to provide a statistically more robust view on the observed convection-  
related { $H_2O$ ,  $\delta D$ } features. For this purpose, we now aim for a multi-annual view on { $H_2O$ ,  $\delta D$ } signals from the June – July  
average clustered for the *non-rain* and *post-rain* events and evaluated for all available data for all three sensors, IASI, AIRS  
260 and TROPOMI (see Table 1). The { $H_2O$ ,  $\delta D$ } pairs collected and clustered for the Guinea Coast and the Sahel are shown in  
Fig. 5, except for TROPOMI over the Guinea Coast (see Fig. 1). The corresponding boxplots for  $H_2O$  and  $\delta D$  of the non- and  
post-rain clusters (shown in Fig. 6) serve to add a more quantitative perspective on the differences between the signals from the

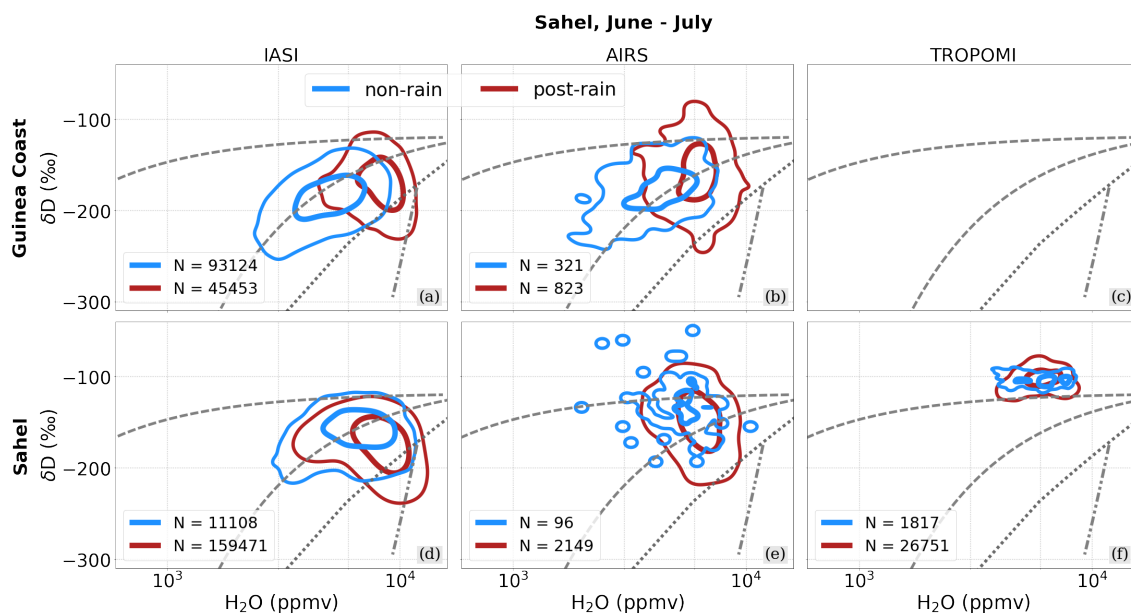


**Figure 5.**  $\{H_2O, \delta D\}$  pair data from IASI and AIRS over the Guinea Coast (a and b) and from IASI, AIRS and TROPOMI over the Sahel (d, e and f) as average for June – July for the respectively available years (see Table 1), clustered into non-rain and post-rain events based on daily averaged precipitation from IMERG and with the contours depicting the distribution of the main 90 % and 50 % scatter points.

two clusters.

It becomes apparent that the characteristic  $\{H_2O, \delta D\}$  signals of the two rain clusters identified for IASI during 2016 (Fig.4) persist as robust feature over the multi-annual perspective for both IASI and AIRS: While the Guinea Coast experiences an overall increase in both  $H_2O$  (around 5 %) and  $\delta D$  (15 – 25 ‰) along the mixing curves, when comparing the non- to post-rain events, the Sahel develops the previously discussed anti-correlated  $\{H_2O, \delta D\}$  features towards the Super-Rayleigh regime as robust response to convective monsoon precipitation (1.5 – 3 % increase in  $H_2O$ , 10 – 25 ‰ decrease in  $\delta D$ ).

In contrast to the vertically resolved data products from IASI and AIRS, TROPOMI does not exhibit such a clear distinction between the non- and post-rain events over the Sahel, but rather experiences a broadening of the  $\{H_2O, \delta D\}$  distribution along the  $\delta D$  dimension. While the average of the  $\delta D$  post-rain boxplot is comparable to the average of the non-rain boxplot (Fig. 6), we observe an increase of the data spread towards both enriching and depleting direction. As TROPOMI  $\delta D$  overall reflects the isotopic composition of the monsoon layer (see Sect. 2.1), we expect contributions from processes enhanced during convection such as surface evapotranspiration and sub-cloud rain evaporation. With the former being associated with enrichment in  $\delta D$  (Noone, 2012; Worden et al., 2021) and the latter with depletion in  $\delta D$  (Risi et al., 2008a; Diekmann et al., 2021a), the hypothesis is that their co-occurrence induces a compensation of their individual effects in the averaged  $\{H_2O, \delta D\}$  pair distribution. Further, as rain evaporation is controlled by the relative humidity of the ambient air, we assume that during the WAM the depletion in  $\delta D$  induced by rain evaporation is less efficient in the boundary layer than in the free troposphere, with the

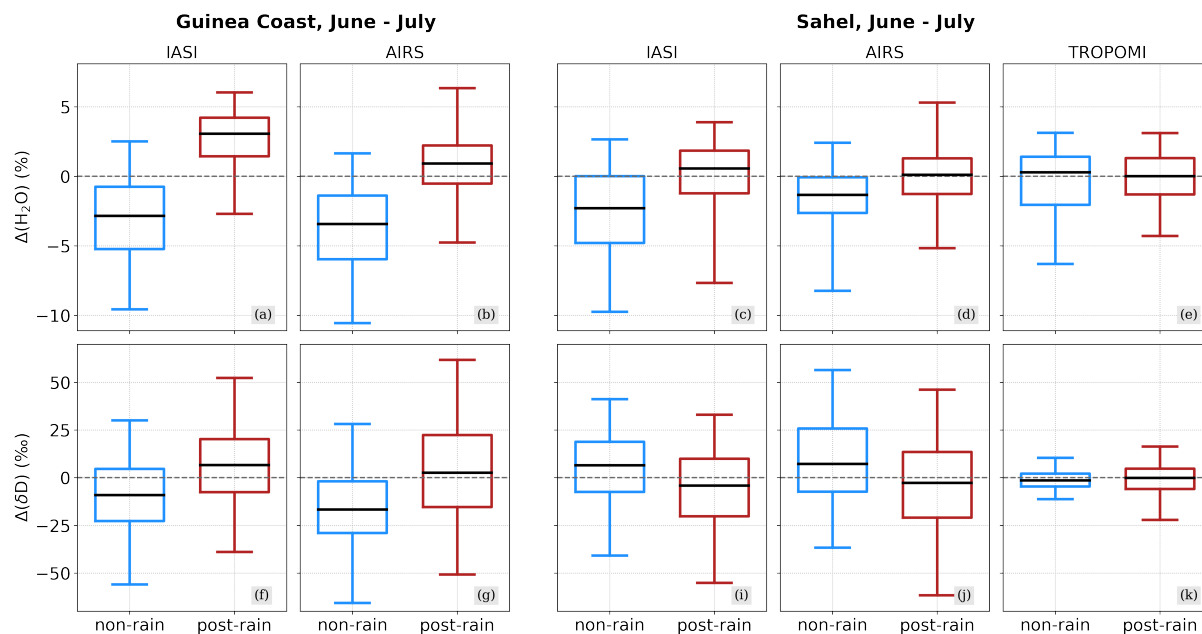


**Figure 6.** Boxplots evaluating the distributions of  $\text{H}_2\text{O}$  and  $\delta\text{D}$  for the non-rain and post-rain clusters during June – July for the respective available years from IASI (a, c, f, i), AIRS (b, d, g, j) and TROPOMI (e, k), see Table 1. The boxes extend from the lower to the upper quartile values with the middle line depicting the median. The whiskers mark the lower and upper 2.5 percentiles. The  $\text{H}_2\text{O}$  (evaluated using the natural logarithm) and  $\delta\text{D}$  values are given as difference to the corresponding instrument-specific average over the full available period (see Table 1).

former being typically moist due to surface evaporation and the latter being exposed to dry air intrusions from the middle and upper troposphere (Diekmann et al., 2021a). Thus, the depleting efficiency of the processes associated with the Super-Rayleigh regime is reduced, what in turn leads to a less pronounced anti-correlation in the  $\{\text{H}_2\text{O}, \delta\text{D}\}$  pairs compared to IASI and AIRS (see Fig. 5).

In conclusion, this section demonstrates that the rather simple and observational-based clustering approach allows to successfully identify observations with and without substantial impact due to convective precipitation, and in addition to clearly distinguish them in the  $\{\text{H}_2\text{O}, \delta\text{D}\}$  phase space in alignment with the characteristic signals due to air mass mixing and microphysical rain-vapour interactions. It underlines that different types of convection and ambient conditions can induce conceptually different effects on the  $\{\text{H}_2\text{O}, \delta\text{D}\}$  phase space. In particular for the free troposphere, a marked anti-correlated relation between increasing  $\text{H}_2\text{O}$  and depleting  $\delta\text{D}$  stands out as result of monsoon convection over the Sahel, where mid-level dry air intrusions into squall line systems induce strong rain evaporation. As, in contrast, the Guinea Coast is not affected by these dry air events, it develops more stable convective systems with reduced rain evaporation efficiency, leading to an overall enrichment in  $\delta\text{D}$  as response to convection over the Tropical Atlantic.

Corresponding results were identified and discussed in the recent study from Galewsky et al. (2023), which investigated tropical



$\delta D$  signals from IASI as a function of the degree of aggregation of the convective systems. They found that highly aggregated convective systems are characterized by mostly moderate precipitation and less pronounced  $\delta D$  depletion in tropospheric water vapour, whereas unaggregated convection (as is the case for the Sahelian squall lines) with strong precipitation is associated with more depleted  $\delta D$  signals.

#### 4 Inter-annual variability of convective $\{H_2O, \delta D\}$ signals during the peak monsoon

In a second step, we investigate, to which extent the short-term convection-related  $\{H_2O, \delta D\}$  features identified on an event basis are observable on a monthly scale comparing different years. For this purpose, we focus on the isotopic signals in the Sahelian mid-troposphere during the peak summer monsoon in August. Figure 7 exhibits the median and data spread for  $H_2O$  and  $\delta D$  from IASI and AIRS as anomalies to the average of all available August data (TROPOMI is omitted due to the limited time coverage) and for precipitation from IMERG.

The first half period, 2015 – 2017, is characterized by a stable median of  $H_2O$  with both IASI and AIRS agreeing with their multi-annual averages. Differences between the two datasets arise with respect to the data spread, which, however, needs to be interpreted carefully, since IASI and AIRS have a considerably different amount of available observations (on average, differing by a factor of 50–200, see Fig. 1) and distributions with smaller samples are more sensitive to outliers. Further, in reasonable agreement between both sensors,  $\delta D$  is enriched between 2015 – 2017 compared to the full period. The annual averages exceed the full period average with up to 20‰ and the upper data spread limits reach up to 60 – 70‰ above average.

The second half of the full period, 2018 – 2020, experiences a marked increase in the precipitation spread. The year 2018 has the highest precipitation median value of the six study years, although  $H_2O$  does not depict a significant deviation from the average. In contrast, the IASI  $\delta D$  shows a consistent drop of around 25‰ compared to 2017 with respect to the median value and data spread. While this decrease in  $\delta D$  is not observed for AIRS during 2018, it becomes even more apparent in 2019, where both sensors indicate a larger depletion in  $\delta D$  compared to 2018. The  $\delta D$  averages reach up to 10‰ below average and the main data spread lays between -100 – 50‰. In addition, strong outliers become apparent for IASI in  $\delta D$  with values far below -100‰, but not in  $H_2O$ , which instead remains in an overall compact and slightly increased data range. This can be understood in the context of the discussion in Sect. 3.1, where convective systems were found to create marked Super-Rayleigh signals through processes like rain evaporation and equilibration, with the effect to reduce  $\delta D$  only. For 2020, IASI again indicates relatively strong depleted  $\delta D$  signals (median below -10‰ and minimum values between -100 to -75‰), but interestingly also  $H_2O$  exhibits comparably low minimum values, while its median value is aligned with the full period average. This can be explained through the corresponding precipitation signals, which similarly show a median value close to the full period median, but also a large extent in the observed data range, reaching from around  $-0.3 \text{ mm}^{-1}$  to over  $0.4 \text{ mm}^{-1}$ . This suggests that 2020 was characterized by both intense convective and dry intrusion events, with the former resulting in humid and depleted and the latter in dry and depleted air masses.

The comparison of the different years underlines that also an anti-correlation between precipitation amount and  $\delta D$  in the vapour phase can be observed. This effect was found to analogously occur for the relation from the precipitation amount

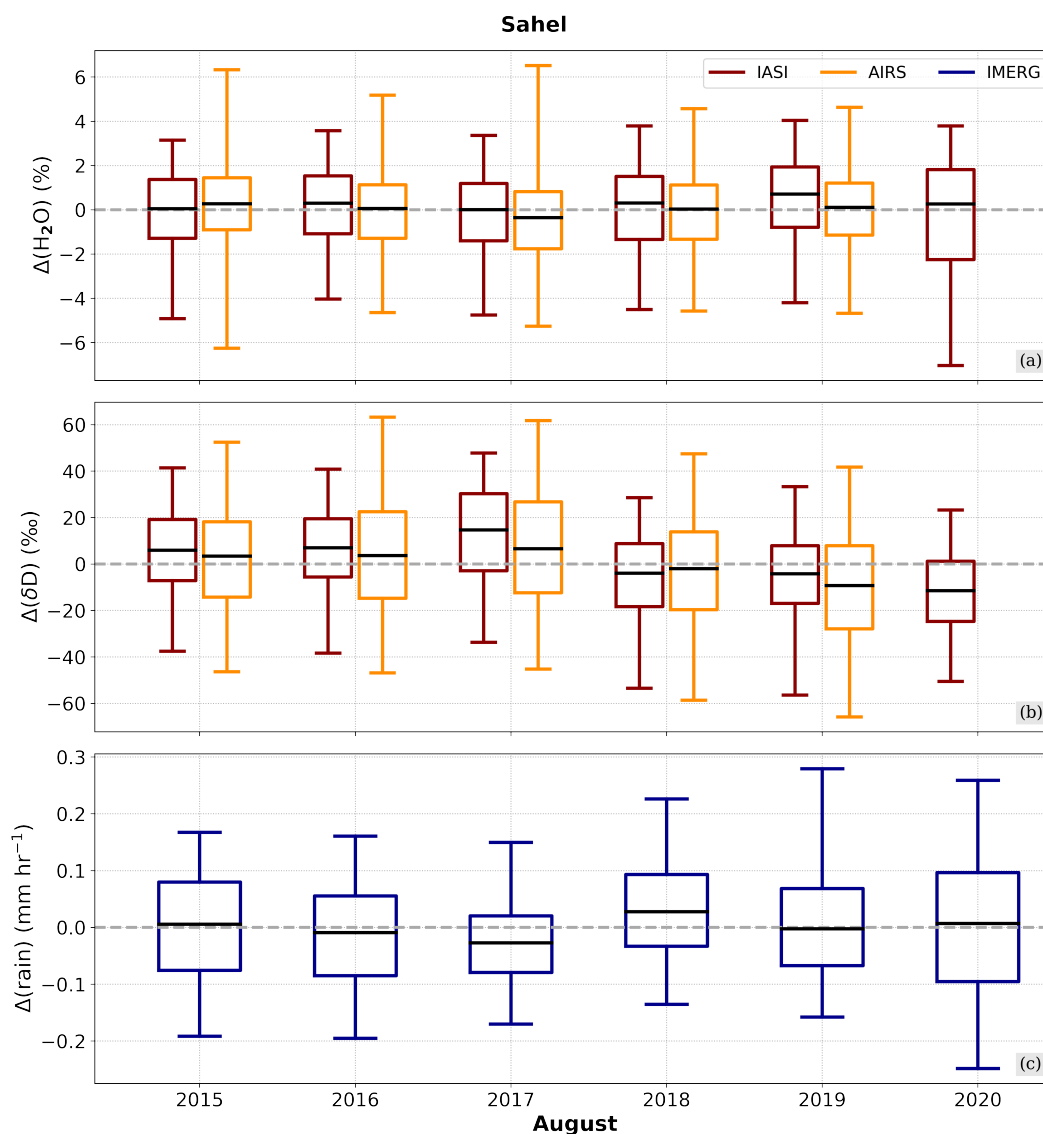


**Figure 7.** Boxplots evaluating the August distributions of  $\text{H}_2\text{O}$  and  $\delta\text{D}$  from IASI and AIRS (red and orange boxes, shown in a, b) and precipitation from IMERG (blue boxes in c). The boxes extend from the lower to the upper quartile with the middle line depicting the median. The whiskers mark the lower and upper 2.5 percentiles. The  $\text{H}_2\text{O}$  (evaluated using the natural logarithm),  $\delta\text{D}$  and precipitation distributions are given as difference to the corresponding instrument-specific average over the full available period (see Table 1).

to precipitation  $\delta\text{D}$  values (e.g. Dansgaard, 1964; Lee and Fung, 2008; Risi et al., 2008a; Tharammal et al., 2017) as well as to water vapour  $\delta\text{D}$  values (Lawrence et al., 2004; Worden et al., 2007; Tremoy et al., 2012, e.g.), the so-called *amount effect*. Various mechanisms have been proposed for explaining this anti-correlation observed in the vapour phase, such as dry mixing due to convective (Risi et al., 2008a) and meso-scale (Kurita, 2013) downdrafts as well as the occurrence of partial rain

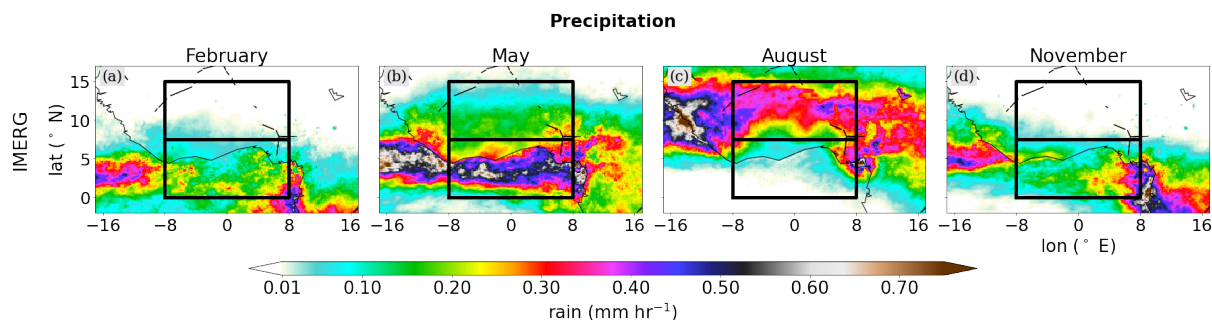


**Figure 8.** Horizontal distributions of monthly averaged precipitation from IMERG over West Africa on the native  $0.1^\circ$  grid. The black rectangles denote the chosen target regions for the Guinea Coast ( $0^\circ$ – $7.5^\circ$  N) and the Sahel ( $7.5^\circ$ – $15^\circ$  N).

330 evaporation (e.g. Worden et al., 2007; Risi et al., 2010b; Noone, 2012), which all have been identified to be pronounced within deep convection (Lacour et al., 2018). In this way, this is consistent with the observed anti-correlation between  $H_2O$  and  $\delta D$  over the Sahel, which, as discussed in Sect.3.1, was found to be the result of intense rain-vapour interactions associated with convective activity.

In conclusion, this section shows that the anti-correlated relation between  $H_2O$  and  $\delta D$  in mid-tropospheric water vapour as a result of Sahelian convection forms a stable signal during the monsoon period. Moreover, we find that the degree of depletion in  $\delta D$  relates to the formation of precipitation events in this region.

## 5 Mean seasonal cycle of $\{H_2O, \delta D\}$ signals

In a third step, we put the seasonal WAM development into a climatological context. The aim is to investigate to which extent the change in circulation and monsoon convection affect the isotopic signature of the tropospheric water vapour over the year and whether further control processes may be identified in the  $\{H_2O, \delta D\}$  phase space.

### 5.1 Seasonality of precipitation

The subject of our discussion is averaged data from February, May, August and November, with these months proving useful of tracking the overall different seasonal cycles in precipitation over the Guinea Coast and the Sahel. Bringing together the evolution of the horizontal precipitation distributions (Fig. 8) and the region-specific precipitation histograms (Fig. 9g, h), we can characterize the selected months as follows:

- During February, when dry Harmattan winds penetrate for south into the Guinea Coastal region, the land mass of West Africa (Sahel) is mostly rain-free and precipitation is largely restricted to a weak zonal band over the Tropical Atlantic (Guinea Coast).



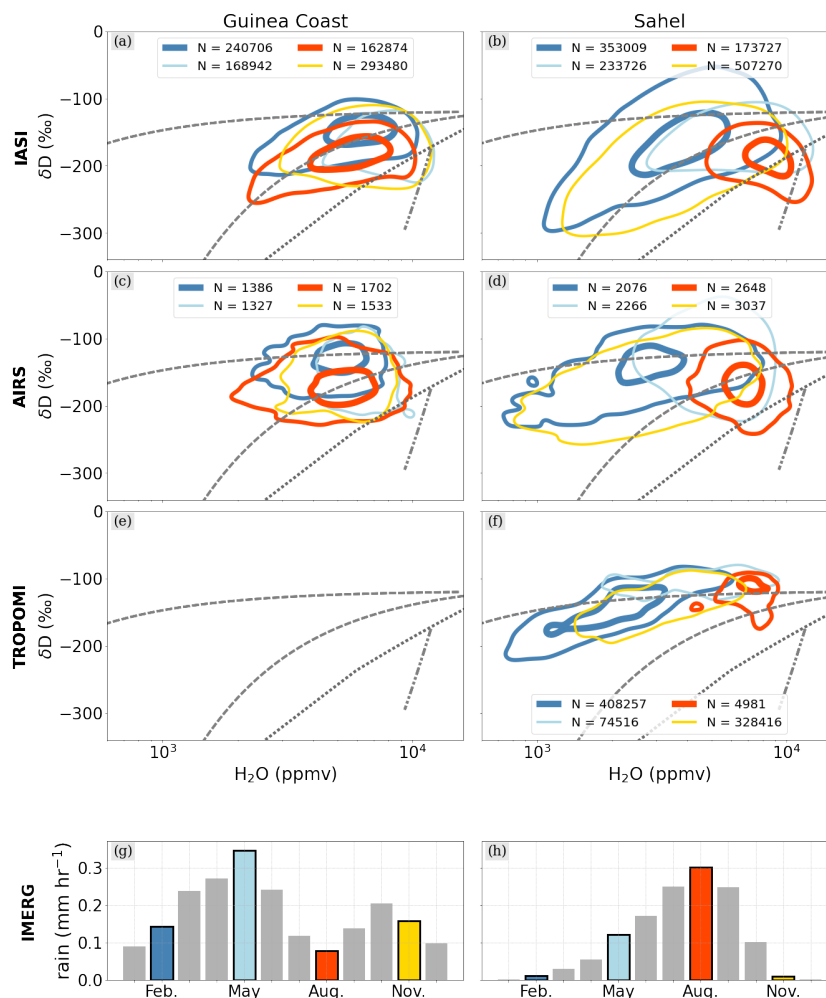


**Figure 9.** First to third row:  $\{H_2O, \delta D\}$  pair distributions from IASI and AIRS for the Guinea Coast (a, c) and from IASI, AIRS and TROPOMI for the Sahel (b and d), averaged for February, May, August and November from the available periods, respectively (see Table 1). The contours indicate the distribution of the main 90 % and 50 % of the respective data points and with the corresponding total data numbers given in the legend. Bottom row: Monthly precipitation averaged over the Guinea Coast and the Sahel. The color-coded bars correspond to the time-periods of the respective contours in (a) and (b).

350

- In May, the precipitation intensifies strongly, though still remains over the ocean. As a result, the Guinea Coast experiences a first rain season and first precipitation events occur over the Sahel.
- In August, the monsoon is fully established and strong southerly winds from the Tropical Atlantic push the precipitation band northwards into the Sahel. While a little dry season develops over the Guinea Coast, the Sahel shows its annual precipitation peak.

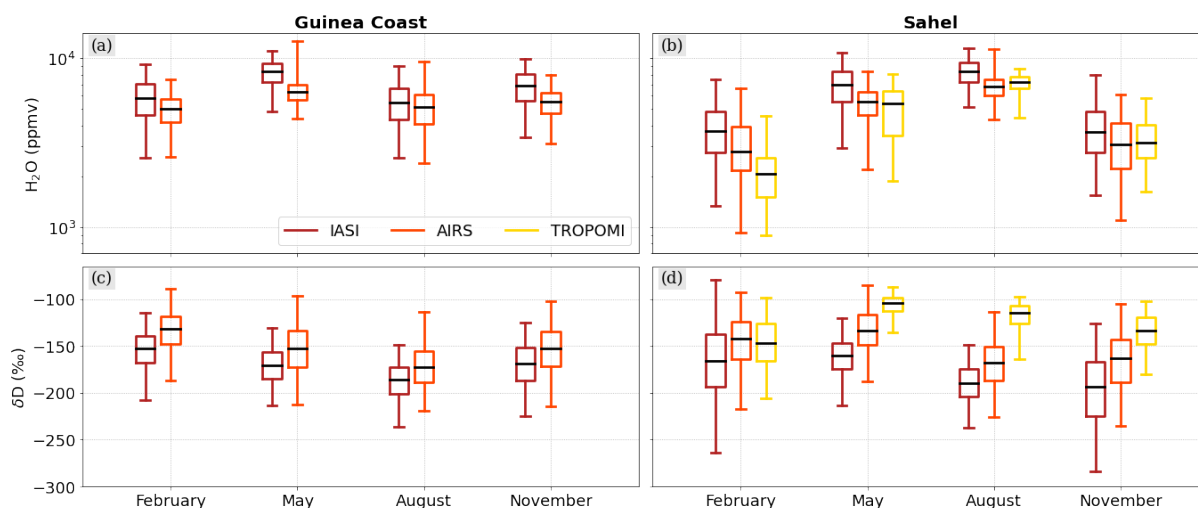


**Figure 10.** Boxplots evaluating the distributions of H<sub>2</sub>O (using the natural logarithm) and δD from IASI, AIRS and TROPOMI for the Guinea Coast (a, c) and the Sahel (b and d), averaged for February, May, August and November from the available periods, respectively (see Table 1). The boxes extend from the lower to the upper quartile with the middle line depicting the median.

– During November, the monsoon has retreated, leading to a distribution largely similar to February. The Sahel is overall dry and the southwards propagation of the precipitation band creates a second, weaker rain season over the Guinea Coast.

In this way, we confirm that the IMERG precipitation products of the selected months serve as a valuable proxy for tracking the mean dynamical cycle over the West Africa. Hence, in the following we investigate the corresponding {H<sub>2</sub>O, δD} pair distributions from IASI, AIRS and TROPOMI (Fig. 9a–f) and the respective boxplots of H<sub>2</sub>O and δD (Fig. 10).

## 5.2 Seasonality of {H<sub>2</sub>O, δD} pairs

In terms of absolute values (Fig. 10), H<sub>2</sub>O from IASI appears consistently higher compared to AIRS, with an averaged difference of around 1000 – 1500 ppmv. For δD, a positive bias by around 15 – 25‰ becomes visible in the AIRS data compared to IASI. The paired {H<sub>2</sub>O, δD} distributions from Fig. 9a–d reflect the overall biases in H<sub>2</sub>O and δD between the two instruments and, additionally, point out a further discrepancy for very dry conditions: In particular during February over the Sahel, AIRS develops strong features towards lower H<sub>2</sub>O values (down to 1000 ppmv) at rather constant δD (slightly below –200‰), where IASI reaches down to –300‰ at the same H<sub>2</sub>O range. Similar patterns were observed by Schneider et al. (2016), when characterizing the impact of applying the harmonization of the vertical sensitivities for the H<sub>2</sub>O and δD retrieval states. Thus, we assume that the here observed discrepancies for very dry conditions between IASI and IARS are result of the missing harmonization step for the AIRS H<sub>2</sub>O and δD products. However, as these differing {H<sub>2</sub>O, δD} features would falsely imply different contributions from underlying control processes (i.e. mixing or Rayleigh processes), we agree with Schneider et al. (2016) to emphasize the necessity of ensuring that retrieved profiles of H<sub>2</sub>O and δD refer to the same vertical atmospheric



layers.

Further, TROPOMI shows a  $\text{H}_2\text{O}$  value range comparable to AIRS (except for February), and in terms of  $\delta\text{D}$ , TROPOMI appears even more enriched on the large scale than IASI and AIRS ( $\delta\text{D}$  increase up to 70‰). This is expected as TROPOMI is a total column product and thus dominated by the lower troposphere, which is typically more enriched due to contributions from e.g. evapotranspiration (Worden et al., 2021). However, the direct comparison of the absolute data range of  $\text{H}_2\text{O}$  and  $\delta\text{D}$  from TROPOMI (total column products) to IASI or AIRS (vertically resolved products) needs to be treated with caution due to the structurally differing vertical sensitivities of the different products.

Throughout the whole year, the Guinea Coast shows relatively high and overall stable signals in  $\text{H}_2\text{O}$  and  $\delta\text{D}$  for both IASI and AIRS (Fig. 9a, c; TROPOMI is not considered for the target domain over the Guinea Coast), and the corresponding  $\{\text{H}_2\text{O}, \delta\text{D}\}$  pair distributions gather around the moist and enriched hyperbolic mixing regime. This is the result of the Tropical Atlantic acting as strong evaporative source of moisture into the troposphere (Frankenberg et al., 2009; Diekmann et al., 2021a). The rain seasons during May and November further moisten the already humid troposphere (up to approx. 10 000 ppmv) and additionally lead to a slight depletion in  $\delta\text{D}$  (down to approx. -200‰). As result to the increased occurrence of rain-vapour interaction during the rain seasons, where in particular rain condensation and evaporation deplete the water vapour in  $\delta\text{D}$ , the respective  $\{\text{H}_2\text{O}, \delta\text{D}\}$  pair distributions depict a minor shift from the mixing regime to the Rayleigh curve and even slightly to the Super-Rayleigh regime. During the dry season between the two rain seasons, the  $\{\text{H}_2\text{O}, \delta\text{D}\}$  pairs show a stretch along the indicated mixing curve down to 2000 ppmv in  $\text{H}_2\text{O}$  and -230‰ in  $\delta\text{D}$ , assumingly as response to dry intrusions mixing into the Guinean troposphere.

In contrast to the  $\{\text{H}_2\text{O}, \delta\text{D}\}$  evolution over the Guinea Coast, drastic differences become evident between the dry winter and rainy summer periods for the study domain over the Sahel, which can be understood in the context of the discussion about the seasonal movement of the precipitation belt (Sect. 5.1). Due to its more northern position, the Sahelian troposphere experiences a stronger dehydration than the Guinea Coast during the dry season (represented here by November and February). With the precipitation maximum being located over the Tropical Atlantic, almost no precipitation occurs over the Sahel. Further, the descending branch of the Hadley cell is found to feed dry and depleted air masses into the North and West African troposphere (Frankenberg et al., 2009), which are then transported by the far-south reaching Saharan Harmattan winds towards the Sahel. With only weak evaporation taking place, this creates a strong mixing signal in the  $\{\text{H}_2\text{O}, \delta\text{D}\}$  distribution of the Sahelian troposphere reaching minimum values of 1000 ppmv for  $\text{H}_2\text{O}$  and -300‰ for  $\delta\text{D}$  for IASI. This is in agreement with Diekmann et al. (2021a), where this moist mixing curve was found to well represent the near-surface moistening along the Harmattan winds and the Atlantic westerly inflow. Similar to the findings over the Guinea Coast, AIRS depicts a similar spread in  $\text{H}_2\text{O}$ , while for  $\delta\text{D}$  an enriched bias in low  $\delta\text{D}$  regimes is documented (see discussions above). This reduces the observed spread in  $\delta\text{D}$ , which varies between -200 and -100‰ over the full  $\text{H}_2\text{O}$  range. For TROPOMI, the column-averaged  $\delta\text{D}$  represents mainly the  $\delta\text{D}$  values of the humid boundary layer (see discussion in Sect. 2.1) and there is only a weak variability, with a data range between -100 and -200‰. The column-averaged  $\text{H}_2\text{O}$  can be interpreted as a measure of the depth of the humid near-surface layer. For a deep humid layer, as it is the case in the monsoon layer over West Africa during the rain season (Cornforth et al., 2017),  $\text{H}_2\text{O}$  values are much higher than for a shallow boundary layer during the dry season. These particularities of the



column-averaged  $\{H_2O, \delta D\}$  pair data create strong signals along the mixing line that arise from the mixing of a humid and a very dry end member.

Even though the Sahelian winter is mostly dry and rain-free, rare but heavy precipitation events may form as response to strong tropical-extratropical interactions between the upper tropospheric wind regimes, the monsoon southerlies and the Saharan Harmattan winds (e.g. Knippertz and Martin, 2005; Knippertz and Fink, 2009; Davis et al., 2013). Occasional northward shifts of the moist southerly winds allow the precipitation belt from the Gulf of Guinea to reach (for boreal winter) unusually high latitudes. This explains the occurrences of high moisture contents even in the dry winter season (up to 10000 ppmv), ultimately resulting in a large variability in the corresponding  $\{H_2O, \delta D\}$  pair distributions of all three satellite products.

The winter distribution of Sahelian  $\{H_2O, \delta D\}$  pairs reveals another interesting feature in the  $H_2O$  range of 2000–8000 ppmv. The corresponding contour exhibits enriched  $\delta D$  values of larger than  $-100 \text{ ‰}$ , i.e. above the shown process curves. This is likely caused by vertical mixing of the very dry sub-tropical free tropospheric air with more humid air of the Saharan boundary layer. This mixing peaks in the dust loaded Saharan air layer. Respective high  $\delta D$  values for this layer have been reported in several studies and using in-situ measurements from ground and aircraft (Dyroff et al., 2015; González et al., 2016) and using data from ground- and space-based remote sensing (Schneider et al., 2015).

As discussed in Sect. 5.1, the monsoon onset is characterised by the shift of maximum precipitation from the Guinea Coast to the Sahel during summer. The precipitation peak over the Sahel during August goes along with a strong increase in  $H_2O$  (data range between 5000–10 000 ppmv), whereas  $\delta D$  shows decreasing tendencies (below  $-200 \text{ ‰}$ ) and points to the previously observed anti-correlation between  $H_2O$  and  $\delta D$ . Figure 9 shows that the enhanced depletion during summer is strongly associated with signals below the Rayleigh prediction and creates  $\{H_2O, \delta D\}$  structures following the Super-Rayleigh line indicated in the figure. These features are also detected by the coarser resolved AIRS dataset, where the anti-correlation is less pronounced but still observable. Furthermore, despite the vertical smoothing over the troposphere for TROPOMI, which leads to a shift of the  $\{H_2O, \delta D\}$  pair contour to higher  $\delta D$  and lower  $H_2O$ , the Super-Rayleigh structures stand out as distinct spike in the otherwise round  $\{H_2O, \delta D\}$  pair contour. This underlines the strong depleting effect of the rain-vapour interactions that mainly occur in a rather shallow layer in the free troposphere (Diekmann et al., 2021a).

In conclusion, we find that the  $\{H_2O, \delta D\}$  data over the Sahel reflect the overall transition from the dry winter season, which is mostly governed by dry air mass mixing, to the summer monsoon season, when moist air reaches into the Sahel and drives microphysical processes related to convection. In contrast, the Guinea Coast develops a comparably less pronounced seasonality in the  $\{H_2O, \delta D\}$  phase space due to its structurally different meteorological conditions. In this way, this section demonstrates that the  $\{H_2O, \delta D\}$  phase space is capable of tracking individual effects from dynamical and microphysical processes that control the atmospheric state over West Africa.

## 6 Conclusion and Outlook

The goal of this study was to characterize the joint variability of  $H_2O$  and  $\delta D$  pairs in the West African troposphere using data from remote sensing and to shed light on the key processes controlling this variability. For this purpose, global and multi-annual



440 data from the state-of-the-art infrared satellite sensors IASI, AIRS and TROPOMI served to track pairs of tropospheric  $\text{H}_2\text{O}$  and  $\delta\text{D}$  abundances over the Guinea Coastal region and the Sahel from the interannual down to the convective scale. Based on IMERG precipitation estimates, we derive a clustering method to distinguish observations affected by deep convection or not. Further, the use of idealized process curves in  $\{\text{H}_2\text{O}, \delta\text{D}\}$  phase space, as derived by the Lagrangian process attribution study in Diekmann et al. (2021a), allowed to interpret the remotely sensed  $\{\text{H}_2\text{O}, \delta\text{D}\}$  pairs with respect to the governing dynamical and microphysical processes.

445 By bringing together the isotopic and precipitation datasets for the Sahel and the Guinea Coast, we were able to derive the following conclusions:

- Despite the rather simple concept of our precipitation-based clustering method, we find that different types of convection lead to different structures in  $\{\text{H}_2\text{O}, \delta\text{D}\}$  phase space during the monsoon: Over the Sahel, where convective squall line events are opposed to strong dry air intrusions, convective precipitation is associated with the coupling of rain condensation and evaporation. As a result, this leads to a moistening of the mid-troposphere as well as to an enhanced depletion in  $\delta\text{D}$ , creating clearly anti-correlated features in the  $\{\text{H}_2\text{O}, \delta\text{D}\}$  phase space towards the Super-Rayleigh regime. In contrast, the Guinea Coast is less affected by dry intrusions, thus here convective precipitation goes along with overall moist and enriched air masses.
- The anti-correlated behaviour between  $\text{H}_2\text{O}$  and  $\delta\text{D}$  over the Sahel during the monsoon peak remains a robust feature in the multi-year perspective. In addition, an anti-correlation between precipitation amount and  $\delta\text{D}$  becomes apparent, where stronger precipitation events are associated with more enhanced  $\delta\text{D}$  depletion, thus pointing towards the amount effect in water vapour.
- The analysis of the mean seasonal cycles demonstrates that the anti-correlated relation between  $\text{H}_2\text{O}$  and  $\delta\text{D}$  is overall limited to the monsoon period and to the Sahel. During the Sahelian winter, which is overall dry and rain-free, predominant mixing signals form as response to strong dynamical processes over West Africa. Again in contrast, the Guinea Coast appears consistently moist and enriched and due to the missing dry air intrusions no significant depletion in  $\delta\text{D}$  develops.

465 The discussed features in  $\{\text{H}_2\text{O}, \delta\text{D}\}$  over the Guinea Coast and the Sahel are particularly pronounced and qualitatively consistent for the vertically resolved water vapour isotope products from IASI and AIRS. Compared to AIRS, IASI reveals a difference of approx. 1000 – 1500 ppmv in  $\text{H}_2\text{O}$  and of approx. 10 – 20‰ in  $\delta\text{D}$ . In contrast, the total-column-averaged TROPOMI product differs markedly from IASI and AIRS. Generally, the seasonal TROPOMI  $\{\text{H}_2\text{O}, \delta\text{D}\}$  cycle is similar to the signals observed by the other instruments, although the anti-correlation between  $\text{H}_2\text{O}$  and  $\delta\text{D}$  associated to Sahelian convection is less evident due to weak  $\delta\text{D}$  variability. This is due to the fact that the TROPOMI  $\text{H}_2\text{O}$  data mainly indicate the depth of the monsoon layer (i.e. high total-column-average  $\text{H}_2\text{O}$  referring to a deep monsoon layer), whereas its  $\delta\text{D}$  reflects the isotopic composition predominantly from within the monsoon layer.

470 In conclusion, this study underlines the strong potential of utilizing paired distributions of  $\text{H}_2\text{O}$  and  $\delta\text{D}$  observed from space to study the atmospheric water cycle and to foster our process understanding associated to tropical convection, microphysical



processes and the large-scale circulation. Together with new frameworks to describe isotopic processes in a more quantitative way (Galewsky et al., 2023), with new methods to combine retrieval results from different instruments in order to create synergy products with increased information content (e.g. for IASI and TROPOMI, see Schneider et al., 2021) and with new techniques to assimilate isotopic observations into atmospheric models (Toride et al., 2021; Schneider et al., 2023), promising opportunities are emerging to further exploit the process-based view of paired  $\{H_2O, \delta D\}$  distributions and, hence, to reveal new insights into atmospheric processes and their numerical representations.

*Data availability.* The MUSICA IASI data are available at <https://doi.org/10.35097/415>. The AIRS data can be accessed at [https://tropes. gesdisc.eosdis.nasa.gov/data/TROPESS\\_Reanalysis\\_Summary/TRPSYL2HD0AIRSORS.1/](https://tropes.480 gesdisc.eosdis.nasa.gov/data/TROPESS_Reanalysis_Summary/TRPSYL2HD0AIRSORS.1/). Information on how to access the TROPOMI data are documented in <https://s5pinnovationh2o-iso.le.ac.uk/elementor-129/>. The GPM IMERG data are available at <https://gpm.nasa.gov/data/directory>.

*Author contributions.* Matthias Schneider, Benjamin Ertl and Christopher Diekmann have created and provided the MUSICA IASI data set, whereby they have been supported by Farahnaz Khosrawi and Frank Hase. Hartmut Boesch and Tim Trent have created and provided the Sentinel-5P data set with support by Amelie Ninja Roehling. John Worden has created and provided the AIRS dataset. Peter Knippertz has provided the scientific background about the West African Monsoon. Peter Knippertz, Matthias Schneider and Christopher Diekmann have designed the concept of the study. All authors supported the generation of the final version of this manuscript.

*Competing interests.* Farahnaz Khosrawi is a member of the editorial board of Atmospheric Chemistry and Physics.

*Acknowledgements.* This work has been financially supported in the context of the projects MOTIV and TEDDY (funded by the Deutsche Forschungsgemeinschaft under project IDs/Geschäftszeichen 950290612604/GZ:SCHN1126/2-1 and 416767181/GZ:SCHN1126/5-1, respectively) and the project Sentinel-5P+Innovation H2O-ISO (funded by the European Space Agency, ESA Contract No. 4000127561/19/INS). Further, it has benefited from the project MUSICA (funded by the European Research Council under the European Community's Seventh Framework Programme (FP7/2007-2013)/ERC Grant Agreement number 256961). The technical processing for the presented results has been performed using the supercomputer HoreKa, which is funded by the Ministry of Science, Research and the Arts Baden-Württemberg and by the German Federal Ministry of Education and Research. Part of this research was carried out at the Jet Propulsion Laboratory, California Institute of Technology, under a contract with the National Aeronautics and Space Administration.



## References

- Barthlott, S., Schneider, M., Hase, F., Blumenstock, T., Kiel, M., Dubravica, D., García, O. E., Sepúlveda, E., Mengistu Tsidu, G., Takele Kenea, S., Grutter, M., Plaza-Medina, E. F., Stremme, W., Strong, K., Weaver, D., Palm, M., Warneke, T., Notholt, J., Mahieu, E., Servais, C., Jones, N., Griffith, D. W., Smale, D., and Robinson, J.: Tropospheric water vapour isotopologue data (H<sub>2</sub>16O, H<sub>2</sub>18O, and HD<sub>16</sub>O) as obtained from NDACC/FTIR solar absorption spectra, *Earth System Science Data*, 9, 15–29, <https://doi.org/10.5194/essd-9-15-2017>, 2017.
- Berntell, E., Zhang, Q., Chafik, L., and Körnich, H.: Representation of Multidecadal Sahel Rainfall Variability in 20th Century Reanalyses, *Scientific Reports*, 8, 10937, <https://doi.org/10.1038/s41598-018-29217-9>, 2018.
- 500 Bielli, S., Douville, H., and Pohl, B.: Understanding the West African monsoon variability and its remote effects: An illustration of the grid point nudging methodology, *Climate Dynamics*, 35, 159–174, <https://doi.org/10.1007/s00382-009-0667-8>, 2010.
- Bolot, M., Legras, B., and Moyer, E. J.: Modelling and interpreting the isotopic composition of water vapour in convective updrafts, *Atmospheric Chemistry and Physics*, 13, 7903–7935, <https://doi.org/10.5194/acp-13-7903-2013>, 2013.
- Clerbaux, C., Boynard, A., Clarisse, L., George, M., Hadji-Lazaro, J., Herbin, H., Hurtmans, D., Pommier, M., Razavi, A., Turquety, S., 510 Wespes, C., and Coheur, P. F.: Monitoring of atmospheric composition using the thermal infrared IASI/MetOp sounder, *Atmospheric Chemistry and Physics*, 9, 6041–6054, <https://doi.org/10.5194/acp-9-6041-2009>, 2009.
- Colman, A., Rowell, D., Foamouhoue, A. K., Ndiaye, O., Rodríguez-Fonseca, B., Suarez, R., Yaka, P., Parker, D. J., and Diop-Kane, M.: Seasonal Forecasting, chap. 8, pp. 289–322, John Wiley & Sons, Ltd, <https://doi.org/https://doi.org/10.1002/9781118391297.ch8>, 2017.
- Cornforth, R., Mumba, Z., Parker, D. J., Berry, G., Chapelon, N., Diakaria, K., Diop-Kane, M., Ermert, V., Fink, A. H., Knippertz, P., Lafore, 515 J. P., Laing, A., Lepape, S., Maidment, R., Methven, J., Orji, B., Osika, D., Poan, E., Roca, R., Rowell, S., Smith, R., Spengler, T., Taylor, C. M., Thorncroft, C., Vincendon, J.-C., Yorke, C., and Thorncroft, C.: Synoptic Systems, chap. 2, pp. 40–89, John Wiley & Sons, Ltd, <https://doi.org/https://doi.org/10.1002/9781118391297.ch2>, 2017.
- Craig, H.: Standard for reporting concentrations of deuterium and oxygen-18 in natural waters, *Science*, 133, 1833–1834, <https://doi.org/10.1126/science.133.3467.1833>, 1961.
- 520 Dansgaard, W.: Stable isotopes in precipitation, *Tellus*, 16, 436–468, <https://doi.org/10.1111/j.2153-3490.1964.tb00181.x>, 1964.
- Davis, J., Knippertz, P., and Fink, A. H.: The predictability of precipitation episodes during the West African dry season, *Quarterly Journal of the Royal Meteorological Society*, 139, 1047–1058, <https://doi.org/10.1002/qj.2014>, 2013.
- de Vries, A. J., Aemisegger, F., Pfahl, S., and Wernli, H.: Stable water isotope signals in tropical ice clouds in the West African monsoon simulated with a regional convection-permitting model, *Atmospheric Chemistry and Physics*, 22, 8863–8895, <https://doi.org/10.5194/acp-22-8863-2022>, 2022.
- 525 Dhonneur, G.: Les amas nuageux mobiles, principale composante de la météorologie du Sahel, *La Météorologie Paris*, 6, 75–82, 1981.
- Diekmann, C. J., Schneider, M., Ertl, B., Hase, F., García, O., Khosrawi, F., Sepúlveda, E., Knippertz, P., and Braesicke, P.: The global and multi-annual MUSICA IASI {H<sub>2</sub>O, δD} pair dataset, *Earth System Science Data*, 13, 5273–5292, <https://doi.org/10.5194/essd-13-5273-2021>, 2021a.
- 530 Diekmann, C. J., Schneider, M., Knippertz, P., de Vries, A. J., Pfahl, S., Aemisegger, F., Dahinden, F., Ertl, B., Khosrawi, F., Wernli, H., and Braesicke, P.: A Lagrangian Perspective on Stable Water Isotopes During the West African Monsoon, *Journal of Geophysical Research: Atmospheres*, 126, e2021JD034895, <https://doi.org/https://doi.org/10.1029/2021JD034895>, e2021JD034895 2021JD034895, 2021b.



- Dyroff, C., Sanati, S., Christner, E., Zahn, A., Balzer, M., Bouquet, H., McManus, J. B., González-Ramos, Y., and Schneider, M.: Airborne in situ vertical profiling of HDO/H<sub>2</sub>O in the subtropical troposphere during the MUSICA remote sensing validation campaign, *Atmospheric Measurement Techniques*, 8, 2037–2049, <https://doi.org/10.5194/amt-8-2037-2015>, 2015.
- 535 Eckstein, J., Ruhnke, R., Pfahl, S., Christner, E., Diekmann, C. J., Dyroff, C., Reinert, D., Rieger, D., Schneider, M., Schröter, J., Zahn, A., and Braesicke, P.: From climatological to small-scale applications: Simulating water isotopologues with ICON-ART-Iso (version 2.3), *Geoscientific Model Development*, 11, 5113–5133, <https://doi.org/10.5194/gmd-11-5113-2018>, 2018.
- Fink, A. H., Vincent, D. G., and Ermert, V.: Rainfall types in the West African Sudanian zone during the summer monsoon 2002, *Monthly Weather Review*, 134, 2143–2164, <https://doi.org/10.1175/MWR3182.1>, 2006.
- 540 Fink, A. H., Engel, T., Ermert, V., Van Der Linden, R., Schneidewind, M., Redl, R., Afesimama, E., Thiaw, W. M., Yorke, C., Evans, M., and Janicot, S.: Mean climate and seasonal cycle, in: *Meteorology of Tropical West Africa: The Forecasters' Handbook*, pp. 1–39, John Wiley & Sons, Ltd, Chichester, UK, <https://doi.org/10.1002/9781118391297.ch1>, 2017.
- Fitzpatrick, R. G., Bain, C. L., Knippertz, P., Marsham, J. H., and Parker, D. J.: The West African monsoon onset: A concise comparison of definitions, *Journal of Climate*, 28, 8673–8694, <https://doi.org/10.1175/JCLI-D-15-0265.1>, 2015.
- 545 Frankenberg, C., Yoshimura, K., Warneke, T., Aben, I., Butz, A., Deutscher, N., Griffith, D., Hase, F., Notholt, J., Schneider, M., Schrijver, H., and Röckmann, T.: Dynamic processes governing lower-tropospheric HDO/H<sub>2</sub>O Ratios as Observed from Space and Ground, *Science*, 325, 1374–1377, <https://doi.org/10.1126/science.1173791>, 2009.
- Gaetani, M., Pohl, B., Douville, H., and Fontaine, B.: West African Monsoon influence on the summer Euro-Atlantic circulation, *Geophysical Research Letters*, 38, n/a–n/a, <https://doi.org/10.1029/2011GL047150>, 2011.
- 550 Galewsky, J., Steen-Larsen, H. C., Field, R. D., Worden, J., Risi, C., and Schneider, M.: Stable isotopes in atmospheric water vapor and applications to the hydrologic cycle, *Reviews of Geophysics*, 54, 809–865, <https://doi.org/10.1002/2015RG000512>, 2016.
- Galewsky, J., Schneider, M., Diekmann, C., Semie, A., Bony, S., Risi, C., Emanuel, K., and Brogniez, H.: The Influence of Convective Aggregation on the Stable Isotopic Composition of Water Vapor, *AGU Advances*, 4, e2023AV000877, <https://doi.org/https://doi.org/10.1029/2023AV000877>, e2023AV000877 2023AV000877, 2023.
- 555 González, Y., Schneider, M., Dyroff, C., Rodríguez, S., Christner, E., García, O. E., Cuevas, E., Bustos, J. J., Ramos, R., Guirado-Fuentes, C., Barthlott, S., Wiegele, A., and Sepúlveda, E.: Detecting moisture transport pathways to the subtropical North Atlantic free troposphere using paired H<sub>2</sub>O- $\delta$ D in situ measurements, *Atmospheric Chemistry and Physics*, 16, 4251–4269, <https://doi.org/10.5194/acp-16-4251-2016>, 2016.
- 560 Huffman, G., Bolvin, D., Nelkin, E., and Tan, J.: Integrated Multi-satellitE Retrievals for GPM (IMERG) Technical Documentation, Tech. rep., NASA Goddard Centre, <https://gpm.nasa.gov/data/imerg>, accessed on 2021-02-15, 2019.
- Huffman, G. J., Bolvin, D., Braithwaite, D., Hsu, K., Joyce, R., and Xie, P.: Integrated Multi-satellitE Retrievals for GPM (IMERG), version 4.4, <https://gpm.nasa.gov/data/directory>, accessed on 2021-02-07, 2014.
- Hulme, M.: Climatic perspectives on Sahelian desiccation: 1973-1998, *Global Environmental Change*, 11, 19–29, [https://doi.org/10.1016/S0959-3780\(00\)00042-X](https://doi.org/10.1016/S0959-3780(00)00042-X), 2001.
- 565 Knippertz, P. and Fink, A. H.: Prediction of dry-season precipitation in tropical West Africa and its relation to forcing from the extratropics, *Weather and Forecasting*, 24, 1064–1084, <https://doi.org/10.1175/2009WAF2222221.1>, 2009.
- Knippertz, P. and Martin, J. E.: Tropical plumes and extreme precipitation in subtropical and tropical West Africa, *Quarterly Journal of the Royal Meteorological Society*, 131, 2337–2365, <https://doi.org/10.1256/qj.04.148>, 2005.





- 570 Knippertz, P., Fink, A. H., Deroubaix, A., Morris, E., Tocquer, F., Evans, M. J., Flamant, C., Gaetani, M., Lavaysse, C., Mari, C., Marsham, J. H., Meynadier, R., Affo-Dogo, A., Bahaga, T., Brosse, F., Deetz, K., Guebsi, R., Latifou, I., Maranan, M., Rosenberg, P. D., and Schlueter, A.: A meteorological and chemical overview of the DACCIWA field campaign in West Africa in June-July 2016, *Atmospheric Chemistry and Physics*, 17, 10893–10918, <https://doi.org/10.5194/acp-17-10893-2017>, 2017.
- Kurita, N.: Water isotopic variability in response to mesoscale convective system over the tropical ocean, *Journal of Geophysical Research* 575 *Atmospheres*, 118, 10,376–10,390, <https://doi.org/10.1002/jgrd.50754>, 2013.
- Lacour, J. L., Risi, C., Worden, J., Clerbaux, C., and Coheur, P. F.: Importance of depth and intensity of convection on the isotopic composition of water vapor as seen from IASI and TES  $\delta D$  observations, *Earth and Planetary Science Letters*, 481, 387–394, <https://doi.org/10.1016/j.epsl.2017.10.048>, 2018.
- Lafore, J. P., Chapelon, N., Diop, M., Gueye, B., Largeron, Y., Lepape, S., Ndiaye, O., Parker, D. J., Poan, E., Roca, 580 R., Roehrig, R., Taylor, C., and Moncrieff, M.: Deep Convection, chap. 3, pp. 90–129, John Wiley & Sons, Ltd, <https://doi.org/https://doi.org/10.1002/9781118391297.ch3>, 2017.
- Lawrence, J. R., Gedzelman, S. D., Dexheimer, D., Cho, H. K., Carrie, G. D., Gasparini, R., Anderson, C. R., Bowman, K. P., and Biggerstaff, M. I.: Stable isotopic composition of water vapor in the tropics, *Journal of Geophysical Research: Atmospheres*, 109, <https://doi.org/10.1029/2003jd004046>, 2004.
- 585 Lee, J. E. and Fung, I.: "Amount effect" of water isotopes and quantitative analysis of post-condensation processes, *Hydrological Processes*, 22, 1–8, <https://doi.org/10.1002/hyp.6637>, 2008.
- Maranan, M., Fink, A. H., Knippertz, P., Amekudzi, L. K., Atiah, W. A., and Stengel, M.: A Process-Based Validation of GPM IMERG and Its Sources Using a Mesoscale Rain Gauge Network in the West African Forest Zone, *Journal of Hydrometeorology*, 21, 729 – 749, <https://doi.org/10.1175/JHM-D-19-0257.1>, 2020.
- 590 Marsham, J. H., Dixon, N. S., Garcia-Carreras, L., Lister, G. M., Parker, D. J., Knippertz, P., and Birch, C. E.: The role of moist convection in the West African monsoon system: Insights from continental-scale convection-permitting simulations, *Geophysical Research Letters*, 40, 1843–1849, <https://doi.org/10.1002/grl.50347>, 2013.
- Nlend, B., Celle-Jeanton, H., Risi, C., Pohl, B., Huneau, F., Ngo Boum-Nkot, S., Seze, G., Roucou, P., Camberlin, P., Etame, J., and Ketchemen-Tandia, B.: Identification of processes that control the stable isotope composition of rainwater in the humid tropical West- 595 Central Africa, *Journal of Hydrology*, 584, 124 650, <https://doi.org/10.1016/j.jhydrol.2020.124650>, 2020.
- Noone, D.: Pairing measurements of the water vapor isotope ratio with humidity to deduce atmospheric moistening and dehydration in the tropical midtroposphere, *Journal of Climate*, 25, 4476–4494, <https://doi.org/10.1175/JCLI-D-11-00582.1>, 2012.
- Noone, D., Galewsky, J., Sharp, Z. D., Worden, J., Barnes, J., Baer, D., Bailey, A., Brown, D. P., Christensen, L., Crosson, E., Dong, F., Hurley, J. V., Johnson, L. R., Strong, M., Toohey, D., Van Pelt, A., and Wright, J. S.: Properties of air mass mixing and humidity in the 600 subtropics from measurements of the D/H isotope ratio of water vapor at the Mauna Loa Observatory, *Journal of Geophysical Research Atmospheres*, 116, <https://doi.org/10.1029/2011JD015773>, 2011.
- Pante, G. and Knippertz, P.: Resolving Sahelian thunderstorms improves mid-latitude weather forecasts, *Nature Communications*, 10, 1–9, <https://doi.org/10.1038/s41467-019-11081-4>, 2019.
- Parker, D. J., Fink, A., Janicot, S., Ngamini, J. B., Douglas, M., Afiesimama, E., Agusti-Panareda, A., Beljaars, A., Dide, F., Died- 605 hiou, A., Lebel, T., Polcher, J., Redelsperger, J. L., Thorncroft, C., and Wilson, G. A.: The Amma radiosonde program and its implications for the future of atmospheric monitoring over Africa, *Bulletin of the American Meteorological Society*, 89, 1015–1027, <https://doi.org/10.1175/2008BAMS2436.1>, 2008.



- Risi, C., Bony, S., and Vimeux, F.: Influence of convective processes on the isotopic composition ( $\delta^{18}\text{O}$  and  $\delta\text{D}$ ) of precipitation and water vapor in the tropics: 2. Physical interpretation of the amount effect, *Journal of Geophysical Research Atmospheres*, 113, <https://doi.org/10.1029/2008JD009943>, 2008a.
- Risi, C., Bony, S., Vimeux, F., Descroix, L., Ibrahim, B., Lebreton, E., Mamadou, I., and Sultan, B.: What controls the isotopic composition of the African monsoon precipitation? Insights from event-based precipitation collected during the 2006 AMMA field campaign, *Geophysical Research Letters*, 35, 1–6, <https://doi.org/10.1029/2008GL035920>, 2008b.
- Risi, C., Bony, S., Vimeux, F., Chongd, M., and Descroix, L.: Evolution of the stable water isotopic composition of the rain sampled along sahelian squall lines, *Quarterly Journal of the Royal Meteorological Society*, 136, 227–242, <https://doi.org/10.1002/qj.485>, 2010a.
- Risi, C., Bony, S., Vimeux, F., Frankenberg, C., Noone, D., and Worden, J.: Understanding the Sahelian water budget through the isotopic composition of water vapor and precipitation, *Journal of Geophysical Research Atmospheres*, 115, 1–23, <https://doi.org/10.1029/2010JD014690>, 2010b.
- Risi, C., Muller, C., and Blossy, P.: Rain Evaporation, Snow Melt, and Entrainment at the Heart of Water Vapor Isotopic Variations in the Tropical Troposphere, According to Large-Eddy Simulations and a Two-Column Model, *Journal of Advances in Modeling Earth Systems*, 13, e2020MS002381, <https://doi.org/https://doi.org/10.1029/2020MS002381>, e2020MS002381 2020MS002381, 2021.
- Risi, C., Muller, C., Vimeux, F., Blossy, P., Védeau, G., Dufaux, C., and Abramian, S.: What Controls the Mesoscale Variations in Water Isotopic Composition Within Tropical Cyclones and Squall Lines? Cloud Resolving Model Simulations in Radiative-Convective Equilibrium, *Journal of Advances in Modeling Earth Systems*, 15, e2022MS003331, <https://doi.org/https://doi.org/10.1029/2022MS003331>, e2022MS003331 2022MS003331, 2023.
- Roehrig, R., Bouniol, D., Guichard, F., Hourdin, F., and Redelsperger, J. L.: The present and future of the west african monsoon: A process-oriented assessment of CMIP5 simulations along the AMMA transect, *Journal of Climate*, 26, 6471–6505, <https://doi.org/10.1175/JCLI-D-12-00505.1>, 2013.
- Schneider, A., Borsdorff, T., aan de Brugh, J., Aemisegger, F., Feist, D. G., Kivi, R., Hase, F., Schneider, M., and Landgraf, J.: First data set of  $\text{H}_2\text{O}/\text{HDO}$  columns from the Tropospheric Monitoring Instrument (TROPOMI), *Atmospheric Measurement Techniques*, 13, 85–100, <https://doi.org/10.5194/amt-13-85-2020>, 2020.
- Schneider, M., Romero, P. M., Hase, F., Blumenstock, T., Cuevas, E., and Ramos, R.: Continuous quality assessment of atmospheric water vapour measurement techniques: FTIR, Cimel, MFRSR, GPS, and Vaisala RS92, *Atmospheric Measurement Techniques*, 3, 323–338, <https://doi.org/10.5194/amt-3-323-2010>, 2010.
- Schneider, M., Barthlott, S., Hase, F., González, Y., Yoshimura, K., García, O. E., Sepúlveda, E., Gomez-Pelaez, A., Gisi, M., Kohlhepp, R., Dohe, S., Blumenstock, T., Wiegeler, A., Christner, E., Strong, K., Weaver, D., Palm, M., Deutscher, N. M., Warneke, T., Notholt, J., Lejeune, B., Demoulin, P., Jones, N., Griffith, D. W., Smale, D., and Robinson, J.: Ground-based remote sensing of tropospheric water vapour isotopologues within the project MUSICA, *Atmospheric Measurement Techniques*, 5, 3007–3027, <https://doi.org/10.5194/amt-5-3007-2012>, 2012.
- Schneider, M., González, Y., Dyroff, C., Christner, E., Wiegeler, A., Barthlott, S., García, O. E., Sepúlveda, E., Hase, F., Andrey, J., Blumenstock, T., Guirado, C., Ramos, R., and Rodríguez, S.: Empirical validation and proof of added value of MUSICA's tropospheric  $\delta\text{d}$  remote sensing products, *Atmospheric Measurement Techniques*, 8, 483–503, <https://doi.org/10.5194/amt-8-483-2015>, 2015.
- Schneider, M., Wiegeler, A., Barthlott, S., González, Y., Christner, E., Dyroff, C., García, O. E., Hase, F., Blumenstock, T., Sepúlveda, E., Mengistu Tsidu, G., Takele Kenea, S., Rodríguez, S., and Andrey, J.: Accomplishments of the MUSICA project to provide accurate,



- 645 long-term, global and high-resolution observations of tropospheric H<sub>2</sub>O,  $\delta$ D pairs - A review, *Atmospheric Measurement Techniques*, 9, 2845–2875, <https://doi.org/10.5194/amt-9-2845-2016>, 2016.
- Schneider, M., Ertl, B., Diekmann, C., Khosrawi, F., Röhling, A., Hase, F., Dubravica, D., García, O., Sepúlveda, E., Borsdorff, T., Landgraf, J., Lorente, A., Chen, H., Kivi, R., Laemmel, T., Ramonet, M., Crevoisier, C., Pernin, J., Steinbacher, M., Meinhardt, F., Deutscher, N., Griffith, D., Velazco, V., and Pollard, D.: Synergetic use of IASI and TROPOMI space borne sensors for generating a tropospheric methane
- 650 profile product, *Atmospheric Measurement Techniques Discussions*, pp. 1–37, <https://doi.org/10.5194/amt-2021-31>, 2021.
- Schneider, M., Ertl, B., Diekmann, C. J., Khosrawi, F., Weber, A., Hase, F., Höpfner, M., García, O. E., Sepúlveda, E., and Kinnison, D.: Design and description of the MUSICA IASI full retrieval product, *Earth System Science Data*, 14, 709–742, <https://doi.org/10.5194/essd-14-709-2022>, 2022.
- Schneider, M., Toride, K., Khosrawi, F., Hase, F., Ertl, B., Diekmann, C. J., and Yoshimura, K.: Assessing the potential of free tropo-
- 655 spheric water vapour isotopologue satellite observations for improving the analyses of latent heating events, *EGUsphere*, 2023, 1–23, <https://doi.org/10.5194/egusphere-2023-1121>, 2023.
- Spencer, R. W. and Braswell, W. D.: How Dry is the Tropical Free Troposphere? Implications for Global Warming Theory, *Bulletin of the American Meteorological Society*, 78, 1097–1106, [https://doi.org/10.1175/1520-0477\(1997\)078<1097:HDITTF>2.0.CO;2](https://doi.org/10.1175/1520-0477(1997)078<1097:HDITTF>2.0.CO;2), 1997.
- Stewart, M. K.: Stable isotope fractionation due to evaporation and isotopic exchange of falling waterdrops: Applications to atmospheric
- 660 processes and evaporation of lakes, *Journal of Geophysical Research*, 80, 1133, <https://doi.org/10.1029/JC080i009p01133>, 1975.
- Sultan, B., Baron, C., Dingkuhn, M., Sarr, B., and Janicot, S.: Agricultural impacts of large-scale variability of the West African monsoon, *Agricultural and Forest Meteorology*, 128, 93–110, <https://doi.org/10.1016/j.agrformet.2004.08.005>, 2005.
- Tharammal, T., Bala, G., and Noone, D.: Impact of deep convection on the isotopic amount effect in tropical precipitation, *Journal of Geophysical Research*, 122, 1505–1523, <https://doi.org/10.1002/2016JD025555>, 2017.
- 665 Toride, K., Yoshimura, K., Tada, M., Diekmann, C., Ertl, B., Khosrawi, F., and Schneider, M.: Potential of Mid-tropospheric Water Vapor Isotopes to Improve Large-Scale Circulation and Weather Predictability, *Geophysical Research Letters*, 48, e2020GL091698, <https://doi.org/10.1029/2020GL091698>, 2021.
- Tremoy, G., Vimeux, F., Mayaki, S., Souley, I., Cattani, O., Risi, C., Favreau, G., and Oi, M.: A 1-year long  $\delta$ 18O record of water vapor in Niamey (Niger) reveals insightful atmospheric processes at different timescales, *Geophysical Research Letters*, 39, L08805, <https://doi.org/10.1029/2012GL051298>, 2012.
- 670 Tremoy, G., Vimeux, F., Soumana, S., Souley, I., Risi, C., Favreau, G., and Oi, M.: Clustering mesoscale convective systems with laser-based water vapor  $\delta$ 18O monitoring in niamey (Niger), *Journal of Geophysical Research*, 119, 5079–5103, <https://doi.org/10.1002/2013JD020968>, 2014.
- Trent, T., Boesch, H., Schneider, M., Diekmann, C. J., and et al.: Sentinel-5p + Innovation (S5P+I) - Water Vapour Isotopologues (H<sub>2</sub>O-ISO) Algorithm Theoretical Basis Document (ATBD), ESA S5P+I Project, 2021.
- 675 Vogel, P., Knippertz, P., Fink, A. H., Schlueter, A., and Gneiting, T.: Skill of global raw and postprocessed ensemble predictions of rainfall over Northern Tropical Africa, *Weather and Forecasting*, 33, 369–388, <https://doi.org/10.1175/WAF-D-17-0127.1>, 2018.
- Wiegele, A., Schneider, M., Hase, F., Barthlott, S., García, O. E., Sepúlveda, E., González, Y., Blumenstock, T., Raffalski, U., Gisi, M., and Kohlhepp, R.: The MUSICA MetOp/IASI H<sub>2</sub>O and  $\delta$ d products: Characterisation and long-term comparison to NDACC/FTIR data,
- 680 *Atmospheric Measurement Techniques*, 7, 2719–2732, <https://doi.org/10.5194/amt-7-2719-2014>, 2014.



- Worden, J., Noone, D., Bowman, K., Beer, R., Eldering, A., Fisher, B., Gunson, M., Goldman, A., Herman, R., Kulawik, S. S., Lampel, M., Osterman, G., Rinsland, C., Rodgers, C., Sander, S., Shephard, M., Webster, C. R., and Worden, H.: Importance of rain evaporation and continental convection in the tropical water cycle, *Nature*, 445, 528–532, <https://doi.org/10.1038/nature05508>, 2007.
- 685 Worden, J. R., Kulawik, S. S., Fu, D., Payne, V. H., Lipton, A. E., Polonsky, I., He, Y., Cady-Pereira, K., Moncet, J. L., Herman, R. L., Irion, F. W., and Bowman, K. W.: Characterization and evaluation of AIRS-based estimates of the deuterium content of water vapor, *Atmospheric Measurement Techniques*, 12, 2331–2339, <https://doi.org/10.5194/amt-12-2331-2019>, 2019.
- Worden, S., Fu, R., Chakraborty, S., Liu, J., and Worden, J.: Where Does Moisture Come From Over the Congo Basin?, *Journal of Geophysical Research: Biogeosciences*, 126, e2020JG006024, <https://doi.org/https://doi.org/10.1029/2020JG006024>, e2020JG006024 2020JG006024, 2021.
- 690 Yoshimura, K., Kanamitsu, M., and Dettinger, M.: Regional downscaling for stable water isotopes: A case study of an atmospheric river event, *Journal of Geophysical Research Atmospheres*, 115, <https://doi.org/10.1029/2010JD014032>, 2010.